












# Gallium-68-NODASA-Functionalized D-Lysine Radiosynthesis and first-line in vitro characterization – a potential PET imaging agent for infection

Christiaan A. Gouws<sup>1</sup> , Tricia Naicker<sup>1</sup> , Janie Duvenhage<sup>3,5</sup> , Beatriz G. de la Torre<sup>2</sup> , Fernando Albericio<sup>2</sup> ,  
Hendrik G. Kruger<sup>1</sup> , Biljana Marjanovic-Painter<sup>4</sup> , Sipho Mdanda<sup>3,5</sup> , Jan Rijn Zeevaart<sup>3,4,5</sup> ,  
Thomas Ebenhan<sup>3,5\*</sup> , and Thavendran Govender<sup>6\*</sup> 

<sup>1</sup>Catalysis and Peptide Research Unit, School of Health Sciences, University of KwaZulu-Natal, Durban, South Africa

<sup>2</sup>School of Chemistry and Physics, University of KwaZulu-Natal, Durban, South Africa

<sup>3</sup>Nuclear Medicine Research Infrastructure NPC, Pretoria, South Africa

<sup>4</sup>Radiochemistry, the South African Nuclear Energy Corporation (Necsa) SOC Ltd, Pelindaba, South Africa

<sup>5</sup>Department of Nuclear Medicine, University of Pretoria, Pretoria, South Africa

<sup>6</sup>Department of Chemistry, University of Zululand, KwaDlangezwa, South Africa

## ABSTRACT

The advancement of new Positron Emission Tomography (PET) radiotracers for differentiating bacterial infections from sterile inflammation is essential for accurate diagnosis and treatment monitoring. D-amino acid-based probes have shown promise for bacterial imaging due to their selective peptidoglycan incorporation. However, host enzyme-mediated racemization of radiolabeled D-amino acids and limited tissue penetration of fluorescence signal of fluorescent D-amino acids limits their *in vivo* performance. Herein, we report the successful chemical synthesis, optimized radiosynthesis, and the required first-line *in vitro* characterization of [<sup>68</sup>Ga]Ga-NDL-1 (NDL = NODASA D-lysine; NODASA = 1,4,7-triazacyclononane-1-succinic acid-4,7-diacetic acid) (the L-isomeric compound, aka. [<sup>68</sup>Ga]Ga-NLL-1 was evaluated in parallel as the control). Robust radiolabeling was achieved within 60 minutes using the optimized radiolabeling method, featuring the consistent production of very good radiochemical yields ( $81.7 \pm 3.2\%$ ), apparent molar activities ( $17.1 \pm 0.8$  GBq/ $\mu$ mol) and with excellent radiochemical purities ( $97.7 \pm 0.5\%$ ), free of <sup>68</sup>Ga-colloids; therefore, deemed suitable for future intravenous administration and micro-PET imaging applications. [<sup>68</sup>Ga]Ga-NDL-1 was highly stable during prolonged incubation in the presence of 1000-times excess of EDTA (>93%) as well as during a 2-hour exposure to plasma (>97%). [<sup>68</sup>Ga]Ga-NLL-1 and [<sup>68</sup>Ga]Ga-NDL-1 showed minimal overall blood cell binding (<12%) or plasma protein binding (<15%). Results justify further investigation of [<sup>68</sup>Ga]Ga-NDL-1 as a potential PET imaging agent of infection.

## KEYWORDS

D-amino acid, peptidoglycan, positron emission tomography, bacterial-specific, radiolabeling, radiochemical characterization, imaging of infection

Received 3 December 2024, revised 12 May 2025, accepted 19 May 2025

## INTRODUCTION

Despite advancements in antibiotic drug discovery and development in the last several decades, bacterial infections remain a major global health risk globally.<sup>1–3</sup> With the increasing emergence of antibiotic-resistant bacteria and the discovery of novel classes of antibiotics almost coming to a standstill, early detection and diagnosis of infections of bacterial origin is crucial to provide patients with optimal care and curb the unnecessary use of antibiotics.<sup>1, 4, 5</sup> However, early diagnosis can be challenging owing to overlapping symptoms caused by infectious and inflammatory conditions, especially in elderly and immunocompromised patients affected by opportunistic, occult, and chronic infections. Conventional diagnostic approaches such as clinical history, physical examination, biopsies and blood cultures, sonar, and simple radiographs may not provide a definitive diagnosis. Thus, more sensitive anatomical imaging studies are recommended, such as Computed Tomography (CT), Magnetic Resonance Imaging (MRI), or molecular/functional imaging studies using nuclear medicine modalities such as Single-Photon Emission Tomography (SPECT) and Positron Emission Tomography (PET). Among these, PET is most frequently used in the diagnostic workup and staging of complicated infectious diseases and in monitoring patient responses to therapy.<sup>6</sup>

PET enables visualisation and quantification of pathophysiological changes associated with infection at the molecular level, even before CT/MRI-detectable anatomical changes occur. PET achieves this

by measuring the distribution and localization of an intravenously injected radiotracer. The radiotracer consists of a biochemically active moiety (vector) that provides target specificity, tagged with a radioisotope that releases a positron, measurable by PET, upon decay. Thus, increased radiotracer localization might be associated with increased targeted molecular activity. To this end, currently available radiopharmaceuticals approved to assist diagnosis of infection, such as radiolabeled white blood cells (WBC), [<sup>18</sup>F]fluorodeoxyglucose ([<sup>18</sup>F] FDG), and [<sup>68</sup>Ga]-citrate do not target bacterial-specific molecular mechanisms, but rather rely on secondary, host-mediated inflammatory molecular responses to visualize infections.<sup>7, 8</sup> More and more initiatives are emphasizing the development of novel radiopharmaceuticals that can directly interact with causative pathogens in order to provide even more effective clinical tools for the diagnosis and prognosis of infectious diseases. Furthermore, they may also serve as research tools to enhance our understanding of the underlying mechanisms of therapeutic performance and the emergence of resistant pathogens.<sup>9–16</sup>

Peptidoglycan (PG) is an extracellular cell wall structure maintained by nearly all bacteria and thus offers various avenues for novel bacterial-specific radiotracer development. One such route is the bacterial use of D-enantiomer amino acids (D-AAAs) as substrates for PG biosynthesis, since these D-AAAs also have no significant role in the biological makeup and metabolism of *Mammalia*.<sup>17–21</sup> PG is a complex meshwork of alternating muramic acid and glucosamine-containing glycan chains cross-linked by short-stem peptides.<sup>22</sup> These stem peptides predominantly contain D-AAAs, such as D-alanine and D-glutamic acid, which are recognized and used by periplasmic

\*To whom correspondence should be addressed  
Email: [thomas.ebenhan@up.ac.za](mailto:thomas.ebenhan@up.ac.za) or [Govenderthav@icloud.com](mailto:Govenderthav@icloud.com)

enzymes, such as L,D-transpeptidases and penicillin-binding proteins, to catalyse peptide crosslinking.<sup>22–26</sup> It has also been demonstrated that these enzymes can incorporate non-canonical D-amino acids (such as D-lysine and D-methionine), and are able to modify PG with highly functionalised/modified D-AAs through either direct incorporation or through D-AA exchange reactions, even if they are conjugated to relatively bulky fluorescent groups.<sup>27–31</sup> Exploitation of this mechanism has produced several commercially available imaging agents, also known as molecular probes, that enable *in situ* spatiotemporal monitoring of PG biosynthesis and regulation. Several examples of commercially available fluorescent D-lysine derivatives used to target and visualize PG assembly *in vitro* and *in situ* are displayed in **Figure 1A**.<sup>29, 31</sup> Furthermore, the indiscriminated utilisation of unnatural D-AAs seems to be conserved throughout the bacterial kingdom, including in clinically relevant pathogens, although the incorporation rates can vary.<sup>27, 31</sup>

Recently, the use of radiolabeled D-amino acids as bacterial-specific nuclear imaging agents targeting PG, has been explored.<sup>32</sup> This includes [<sup>14</sup>C]D-methionine and [<sup>14</sup>C]D-alanine which enables the detection and differentiation of actively growing *Escherichia coli*, *Staphylococcus aureus*, and *Pseudomonas aeruginosa* infections from sterile inflammation in murine infection models.<sup>33–36</sup> Furthermore, in initial studies on patients with suspected prosthetic joint infections, [<sup>14</sup>C]D-methionine performed well in the identification of active infections. However, the short half-life of carbon-11 (20.4 min), its associated high cost, and limited availability remain major drawbacks. Additionally, host-mediated racemization of L-isomers and metabolism through D-amino acid oxidase activity have been reported to lead to high radiotracer retention in the liver.<sup>33, 36, 37</sup> Whilst longer-lived fluorine-18-labelled analogues (110.2 min) of D-alanine and D-glutamate have been reported, significant *in vivo* defluorination and lack of homology between native and fluorine-18-analogues have been limiting their further usage.<sup>38, 39</sup> With promising initial results using [<sup>14</sup>C]D-AAs as radiotracer vectors, there has been a quest for the development of 2<sup>nd</sup> generation D-AA-derived radiotracers that utilise alternative radionuclides to mitigate the limitations attributed to the radiochemistry of carbon-11.<sup>39</sup>

Based on the maintenance of PG incorporation by D-AAs modified with relatively bulky fluorophores (**Figure 1A**), we sought to functionalize lysine with 1,4,7-triazacyclononane-1-succinic acid-4,7-diacetic acid (NODASA) to form the individual stereoisomers, NODASA-L-Lysine (NLL-1) and NODASA-D-Lysine (NDL-1) (**Figure 1B**). Functionalization of lysine with NODASA, a macrocyclic bifunctional chelator, should enable efficient chelation of PET-compatible metal radionuclides, such as Gallium-68 (Ga-68).<sup>40, 41</sup> Additionally, NODASA chemistry affords relatively easy conjugation to a targeting vector.<sup>42</sup> Importantly, Ga-68-NODASA radiocomplexes show high radionuclide stability, and the half-life of Ga-68 (67.7 min) matches well with the biological half-lives of most small biomolecules.<sup>41</sup> Also, daily Ga-68-chloride radioactivity is conveniently available in solution by ‘milking’ a germanium-68/gallium-68 generator, a cost-efficient process featuring a facile, on-demand radioactivity production.

The α-amino group of D-amino acids plays a critical role in its biochemical interactions with PG biosynthetic enzymes.<sup>25, 26, 29</sup> In this case, the functionalization does not impact the stereochemistry at the α-amino group and the configuration of D- or L-lysine is retained. The purpose is not to replicate every function of natural lysine, but to retain the essential aspects necessary for PG incorporation.

Herein, we report the successful conjugation of D-lysine and L-lysine to NODASA (NDL, targeting agent; NLL, biological negative control), followed by the development and optimization of the synthesis of Ga-68-radiotracers, [<sup>68</sup>Ga]Ga-NDL-1 and [<sup>68</sup>Ga]Ga-NLL-1, for initial radiopharmaceutical and a first-line *in vitro* characterization as PET imaging agents. Results from this study will aid in justifying the validity of [<sup>68</sup>Ga]Ga-NDL-1 for preclinical assessment as a prospective radiotracer for PET imaging of infection.

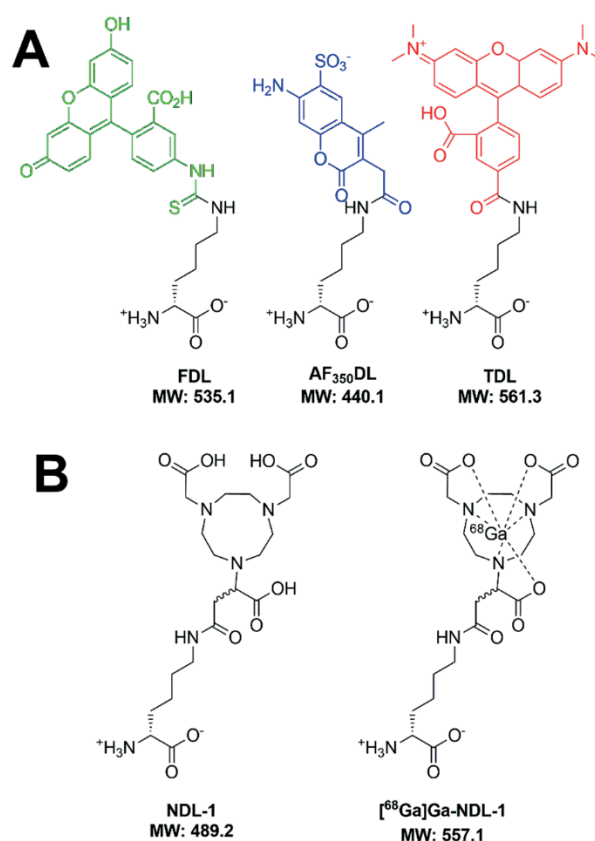


**Figure 1:** (A) Chemical structures and molecular weight (MW, Daltons) of three examples of commercially available fluorescent D-lysine derivatives used for targeting PG *in vitro* and *in situ*.<sup>29, 31</sup> (B): Chemical structure of 1,4,7-triazacyclononane-1-succinic acid-4,7-diacetic acid (NODASA)-functionalized D-lysine (NDL-1) and the corresponding <sup>68</sup>Ga-radioconjugate.

## EXPERIMENTAL

### Syntheses

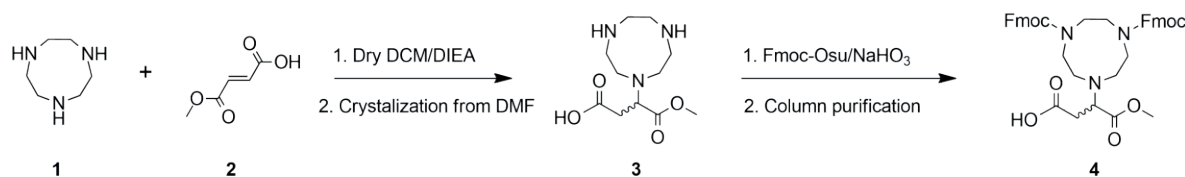
#### Synthesis of NDL and NLL

A procedure developed by Dutta *et al.*<sup>43</sup> for synthesising NODASA-functionalized peptides on resin was modified to functionalise D-lysine and L-lysine with NODASA (**Scheme 1**). More detailed information regarding the synthesis steps is provided in the supplementary information. All synthetic intermediates and products were characterised using a PDA-coupled LCMS (Shimadzu 2020 UFLC-MS, Japan) with a YMC-Triart C18 (5 μm, 4.6 × 150 mm) column. NDL and NLL were isolated by diethyl ether precipitation to form a fine white or off-white powder. The identities of the final NDL and NLL products were confirmed by HRMS-TOF (ESI+); calculated for C<sub>20</sub>H<sub>35</sub>N<sub>5</sub>O<sub>9</sub> [M+H]<sup>+</sup> 490.2508; found 490.2456 (NDL) and 490.2503 (NLL), respectively (**Figure S5**). As discussed in the synthesis results section and **Supplementary Scheme S1**, the final NDL and NLL products each constitute two structural isomers, most probably because of an aspartimide side reaction, and will be referred to as NDL-1/NDL-2 and NLL-1/NLL-2.

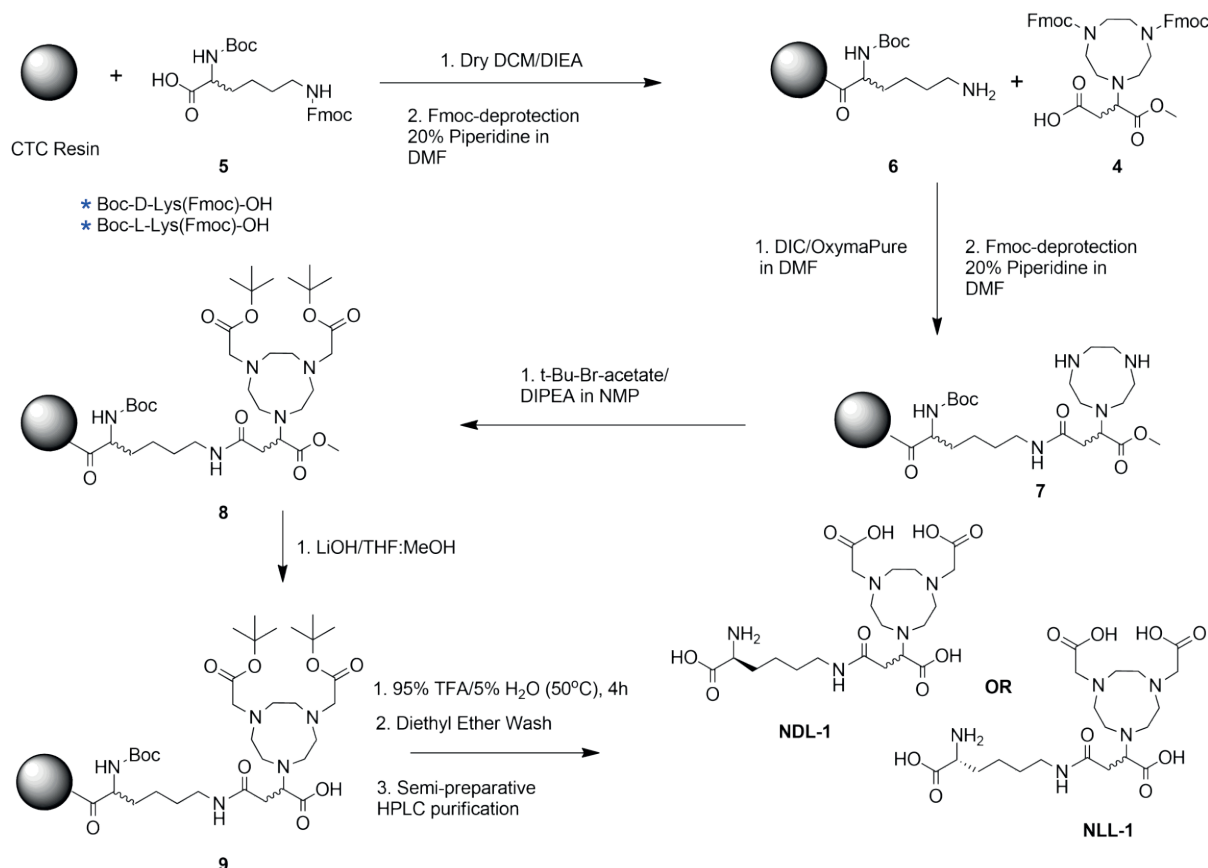
#### NDL-1/2 and NLL-1/2 semi-preparative HPLC separation, purification and analysis

Following synthesis, the respective NDL and NLL structural isomers were successfully separated and purified using a semi-preparative HPLC system (Shimadzu, Kyoto, Japan) coupled to an ACE C18 preparative column (150 × 21.2 mm) using 0.1% TFA in water as Mobile-phase A and 0.1% TFA in acetonitrile as Mobile-phase B. A gradient of 0–10 % Mobile-phase B over 30 min with a flow rate of 10 mL/min was used with PDA detection set at 200nm and 220nm, respectively.

### Step 1: Synthesis of Fmoc-Chelator Precursor



### Step 2: Resin loading and Fmoc-chelator precursor coupling



**Scheme 1:** NDL-1 and NLL-1 synthesis.

NDL-1/NLL-1 eluted at a retention time of 16.3 – 17.0 min, whilst NDL-2 and NLL-2 eluted at 18.3 – 20.8 min. The collected fractions were characterised by LCMS identification of the desired product *m/z* (490.2) and chromatographic purity. Fractions with purity >95% were combined, followed by removal of residual acetonitrile *in vacuo* and freezing at -80°C. Subsequent freeze-drying yielded a white or clear crystalline product.

#### Preparation of the non-radioactive Ga-NDL-1 reference compound

NDL-1 was complexed with gallium(III)chloride (non-radioactive Ga) as follows: 200 µl of 20mM GaCl<sub>3</sub> dissolved in 0.6M HCl was diluted with 400 µl 0.6M HCl and mixed with 240 µl of a 2.5 M sodium acetate solution (pH 4-5). Next, 100 µl 20.0mM NDL-1 (0.5 equiv. to Ga) was added, followed by incubation at room temperature for 15 min.

#### Ga-68 radioactivity production and preparation

A tin-dioxide germanium-68(<sup>68</sup>Ge)/gallium-68(<sup>68</sup>Ga)-generator (iThemba LABS, Somerset West, South Africa) was used to obtain <sup>68</sup>Ga for radiolabeling by using an 0.6M HCl elution fractionation method,<sup>46</sup>

the first 1.0 ml eluate is discarded into a waste vial. The next 2.0 ml eluate, which contains the majority of <sup>68</sup>Ga-activity, is collected (into a separate vial) for use in radiolabeling reactions. The generator line was then rinsed with 7.0 ml into the waste vial. The radioactivity of both the eluate and waste fractions was measured using a CRC Capintec 15 beta dose calibrator (CM Nuclear Systems, Orange Grove, Johannesburg, RSA). Without further purification, the <sup>68</sup>Ga-eluate acidity) was adjusted to pH 4-5 using 2.5M sodium acetate trihydrate, and used for radiolabeling experiments.

#### Radio-HPLC methods for NDL/NLL characterization and radio-analysis

Two different radio-HPLC systems (and their respective developed methods) were used to assess radiochemical purity (%RCP) and radiochemical yields (%RCY) for logistical reasons (Table 1). The HPLC instrumentation used for radioanalysis included an Agilent 1200-series (System 1) or Agilent 1260 Infinity II (System 2), both coupled to a Diode Array Detector and radioactive detector (Socle 2 GABI Nova, Raytest, Straubenhardt, Germany). The samples were injected without prior purification. However, when working with methanol or ethanol,



**Table 1:** Respective radio-HPLC methods used to analyse [<sup>68</sup>Ga]Ga-NDL-1 and [<sup>68</sup>Ga]Ga-NLL-1 radiochemical purity (RCP)

M	Stationary phase (type / dimension)	Mobile phase (cont.0.1% TFA)	Flow (mL/min)	Method gradient	PR* (min)	Free- <sup>68</sup> Ga retention (min)
1	Poroshell 120 EC-C18 2.7µm 3.0 x 150 mm	A: H <sub>2</sub> O B: acetonitrile	0.50	0%B to 5%B in 7 min	2.60 – 2.85	1.30 – 1.40; 1.40 – 2.40 ‡
2	Zorbax SB RP C-18 5µM 4.6 x 250 mm	A: H <sub>2</sub> O B: acetonitrile	1.00	0%B to 7%B in 10 min	6.00 –7.50	3.30–3.80; 5.40–5.80 ‡

Footnotes: **M**) HPLC method; **\***) product retention time; **‡**) Separation of free (uncomplexed) gallium into two peaks can be observed and is common phenomenon reported in literature, especially when using low-gradient elution profiles for reverse-phase chromatography. It has been proposed that such behaviour can be attributed to the existence of different <sup>68</sup>Ga ionic forms, some of which are retained at the head of the reverse-phase column.<sup>54</sup>

the samples were thoroughly dried and resuspended in water before injection to avoid significant changes in retention time (*R<sub>T</sub>*) and peak shape. A wash phase consisting of 95% acetonitrile for 5 min was performed after the gradient, followed by 5 min of re-equilibration.

### Characterization of radiolabeled NDL-1 and NLL-1

For radio-HPLC characterization, initial radiolabeling of NDL-1 and NLL-1 was performed using a 100µM ligand concentration at room temperature for 20 min and generator-produced, buffered <sup>68</sup>Ga-activity prepared as previously described. Radio-characterisation was performed using radio-HPLC method 1, as described in **Table 1**. Confirmation of non-radioactive Ga-NDL-1/-NLL-1 (reference compound) *m/z* and purity was performed using LCMS (Agilent Technologies Inc., Wellington, DE, USA) coupled with a diode array detector using both HPLC methods specified in **Table 1**. Then, the identity of the radioactive [<sup>68</sup>Ga]Ga-NDL-1/NLL-1 was confirmed by comparing peak retention times observed in the radio-chromatogram with the peak retention times observed in the UV-chromatogram of the non-radioactive Ga-NDL-1 reference standards.

### Development and evaluation of optimal radiolabeling parameters

Reaction series were performed in Eppendorf 1.5 mL plastic tubes using 0.225 ml aliquots of generator-produced, buffered <sup>68</sup>Ga-radioactivity (~20.0 MBq). The series of reactions were performed at either pH 3.5 or pH 4.5. The percentage radiochemical yield (%RCY) of each reaction was measured using radio-HPLC method 1. A set of maximum 12 reactions was performed from a single gallium generator elution; every data point represents an independent reaction.

### Proposed NDL-tailored SPE purification method

No previous method was cited by literature, and different SPE cartridge sorbent types were screened. Following that, a Sep-Pak Silica SPE cartridge (Waters Corporation, USA) was used to purify [<sup>68</sup>Ga]Ga-NDL-1/-NLL-1 as follows: 1) before sample loading, the SPE cartridge was pre-conditioned with 2.0 ml water, followed by 10.0 ml EtOH; 2) the radiolabeling reaction solution was diluted with 9.0 ml EtOH (1:9 water/EtOH, v/v) and slowly loaded onto the cartridge material (flow approx. 0.5 mL/min); 3) the reaction vial was washed with 2.0 ml 1:9 water/EtOH and the additional volume loaded onto the cartridge; 4) different gradient elution profiles were established using increasing water/EtOH (v/v) solutions to achieve gradual radioconjugate desorption. Desorption was monitored by measuring the activity retained on the cartridge after each elution fraction, using a CRC Capintec 15 beta dose calibrator. The percentage of captured activity was calculated after each elution fraction as cartridge activity divided by the total loaded activity measured after radiolabeled product loading.

### Evaluating the radiolabeling performance of the optimized radiosynthesis protocol

Radiolabeling was performed several times using the proposed optimized radiosynthesis protocol, with the inclusion of SPE purification

(*n* = 3 for [<sup>68</sup>Ga]Ga-NDL-1 and [<sup>68</sup>Ga]Ga-NLL-1, respectively) to calculate key performance parameters. Radiosynthesis was performed in 10 mL clear borosilicate glass vials. The activity involved before and after each radiosynthesis and SPE purification step was measured using a CRC Capintec 15 beta dose calibrator. The %RCY for the crude radiolabeled product and final %RCP of the SPE-purified radiolabeled products were calculated using radio-HPLC (Method 2). An aliquot of the crude radiolabeled product was taken before SPE purification for %RCY calculation. To calculate the SPE desorption rate, decay-corrected %RCY, loss to apparatus/materials, and the sum of recovered radioactivity, the measured activity fractions were decay-corrected to the time of loading the crude radiolabeled product onto the SPE cartridge.

### Challenge and stability studies

The ability of the produced [<sup>68</sup>Ga]Ga-NDL-1/-NLL-1 to safely complex and sustain <sup>68</sup>Ga-chelation was studied under various conditions by adopting the method used by Dutta *et al.*<sup>43</sup> Briefly, the radiochemical stability of [<sup>68</sup>Ga]Ga-NDL-1/-NLL-1 was measured up to 180 min post-labelling and setting the following challenges: a) the final product solution (as is) was kept at laboratory bench-top conditions; b) product re-formulation and incubation in 0.1M PBS (pH 7.5); and c) product exposure to 1000-fold molar excess of EDTA (pH 7.4 using 1.0 M NaOH); settings b) and c) were incubated at 37°C. At the relevant time points, an aliquot of the sample was analysed using radio-HPLC to determine its relative stability (change in %RCP over time; [<sup>68</sup>Ga]Ga-NDL-1 → radio-HPLC method 1; [<sup>68</sup>Ga]Ga-NLL-1 → radio-HPLC method 2). The results were expressed as % intact radioconjugate normalized to the initial %RCP for each radiolabeled product used in the experiment. Each data point represents a single reaction.

### Physico-chemical characterization (logD<sub>7.4</sub>)

The lipophilicity of [<sup>68</sup>Ga]Ga-NDL-1 and [<sup>68</sup>Ga]Ga-NLL-1 were determined using an *n*-octanol/PBS (pH 7.4) system test, as described by Shi *et al.*<sup>71</sup> Each radioconjugate was diluted with PBS (pH 7.4). For the test, 1.0 ml of radioconjugate/PBS solution (~12 MBq) was mixed with 1.0 ml *n*-octanol and vortexed for 1 min. The mixture was separated by centrifugation at 4500 rpm for 5 min. A 900µl aliquot was aspirated from each layer and transferred into separate Eppendorf tubes. Radioactivity for each phase was determined using a well-type CRC Capintec 15 beta dose calibrator. The LogD<sub>7.4</sub> of each sample (*n* = 3) was calculated as log (*k<sub>o/w</sub>*), the logarithm of the ratio of decay-corrected activity between the octanol and water layers (*k<sub>o/w</sub>*).

### Proteolytic stability and blood distribution assays

Blood samples were collected in heparinised vacutainer tubes kindly provided by the Nuclear Medicine Research Department at the University of Pretoria. All the samples were kept on ice until further use. Plasma samples were obtained by centrifugation at 4000rpm for 2 min (LCEN-401P digital clinical centrifuge, MRC Laboratory Equipment). For all experiments, vials containing blood, plasma, or serum were preheated to 37°C for 5 min before the addition of the

$^{68}\text{Ga}$ -radioconjugate (i.e. the  $^{68}\text{Ga}$ -NDL-1 /or -NLL-1 products with  $\geq 95\%$  RCP were prepared by routine radiosynthesis, as described in the previous section). Before adding to plasma, the pH of the radiolabeled products was adjusted to 7–8 using 1.0M NaOH. Assays were performed using sterile Eppendorf tubes.

Enzymatic plasma stability was determined according to the method described by Xia *et al.*<sup>72</sup> Briefly, each radiolabeled product ( $\sim 10\text{MBq}$ ) was added to 1.0 mL plasma and mixed gently. The solution was incubated at  $37^\circ\text{C}$ . At certain timepoints (0, 30, 60, and 120 min), an aliquot of 200  $\mu\text{L}$  was taken and mixed with 1.0 mL absolute ethanol to precipitate plasma contents. The suspension was separated by centrifugation at 4500 rpm for 5 min. A 100  $\mu\text{L}$  aliquot of the supernatant was taken for radio-HPLC analysis (method 1) and first prepared by evaporating ethanol, followed by resuspension in 100  $\mu\text{L}$  water and injection into the HPLC. The results were expressed as % intact radioconjugate relative to the administered radioconjugate %RCP ( $n=2$ ).

Blood cell association studies were performed as described by Shi *et al.*<sup>71</sup> Each radioconjugate ( $\sim 5.0\text{MBq}$ ) was added to a 1.2 mL whole-blood cell sample, gently mixed, and incubated at  $37^\circ\text{C}$ . At certain timepoints (0, 30, and 60 min), a 300  $\mu\text{L}$  aliquot was transferred to a yellow BD Vacutainer<sup>®</sup> blood collection tube (containing the clot activator/polymer gel). This tube was centrifuged at 4500 rpm for 2 min to separate the serum from the blood cells, which were absorbed into the gel layer. The serum was rinsed into separate tubes using PBS ( $3 \times 0.5\text{ mL}$ ). Radioactivity in both tubes was measured separately using an automated gamma counter (LabLogic, Hidex AMG, Turku, Finland). Blood cell association was calculated by dividing the total radioactivity measured in the blood collection tube with the combined activity of both tubes (decay corrected;  $n = 3$ ).

Serum protein binding assay was performed as described by Mdlophane *et al.*<sup>73</sup> Briefly, each radiolabeled product ( $\sim 1.5\text{MBq}$ ) was added to 500  $\mu\text{L}$  of plasma, gently mixed, and incubated at  $37^\circ\text{C}$ . At certain time points (0, 30, and 60 min), an aliquot of 100  $\mu\text{L}$  was added to 500  $\mu\text{L}$  absolute ethanol to precipitate the plasma contents. The protein precipitate was pelleted by centrifugation at 4500 rpm for 5 min. The pellet was further washed with 500  $\mu\text{L}$  of absolute ethanol, and the supernatants were combined. Radioactivity was measured in the pellet and supernatant using an automated gamma counter (LabLogic; Hidex AMG, Turku, Finland). The percentage of serum protein binding was calculated by dividing the pellet-measured activity by the combined activity of the pellet and supernatant (decay corrected;  $n = 3$ ).

## Statistical Analysis

All data processing calculations were performed using Microsoft Office, Excel Version 2016. Results for  $\text{LogD}_{7.4}$ , percentage of blood cell-associated activity, and percentage of serum protein-bound activity are presented as mean  $\pm$  SD. For blood cell association and serum protein binding results, statistical significance between sample groups per time point of the respective  $^{68}\text{Ga}$ -NDL-1 and  $^{68}\text{Ga}$ -NLL-1 experiments was calculated using one-tailed Student's *t*-test. A two-tailed *t*-test was used to compare the  $^{68}\text{Ga}$ -NDL-1 and  $^{68}\text{Ga}$ -NLL-1. Statistical significance was set at  $P < 0.05$ .

## RESULTS AND DISCUSSION

### Chemical synthesis of NDL-1 and NLL-1

Both NDL-1 and NLL-1 were successfully synthesized in sufficient quantities and purities using a solid-phase peptide synthesis (SPPS) procedure (Scheme 1).<sup>43</sup>

The off-resin production of (4) was successful, yielding a white powder product in 78% yield. Photodiode array (PDA) detector coupled ESI-LCMS showed a single peak ( $>98\%$  pure, UV detection at 300 nm), correlating with the protonated molecular ion of desired product 4,  $m/z$  704 ( $[\text{MH}]^+$ ) (Figure S1).

2-Chlorotriptyl chloride (CTC) resin was preloaded with commercially available Boc-D-Lys(Fmoc)-OH and Boc-L-Lys(Fmoc)-OH (5), respectively. Following Fmoc deprotection, the deprotected primary amine situated on the lysine side chain of 6 was amidated with Fmoc-protected 4-methoxy-4-oxo-3-(1,4,7-triazonan-1-yl) butanoic acid (4), as confirmed by the LCMS analysis of an aliquot of cleaved resin (Figure S2). Two HPLC peaks correlating with the protonated molecular ion of the desired amide,  $[\text{M}+\text{H}]^+$ ,  $m/z$  932, and the Boc-deprotected amine,  $[\text{M}-\text{Boc}+\text{H}]^+$  with  $m/z$  832, were observed. Following Fmoc deprotection to yield 7, on-resin alkylation of the triazacyclononane amine groups with *tert*-butyl bromoacetate was performed to successfully produce 8. PDA-coupled ESI-LCMS analysis of an aliquot of the resin cleaved under mild conditions (Figure S3) revealed two HPLC peaks (retention times, RT, 13.8 min and 18.2 min) correlating with the protonated molecular ion and daughter ions of the desired product, 8, (ESI-MS)  $m/z$  504 ( $[\text{M}-\text{Boc}-2\text{tBu}+\text{H}]^+$ ) ( $R_T$  13.8 min), and the second peak ( $R_T$  18.2 min) corresponding to  $m/z$  716 ( $[\text{M}+\text{H}]^+$ ), 616 ( $[\text{M}-\text{Boc}+\text{H}]^+$ ), 560 ( $[\text{M}-\text{Boc}-\text{tBu}+\text{H}]^+$ ). The combined peaks indicate  $>98\%$  conversion to the desired product (8).

At this point, it should be noted that significant amounts of a by-product, most probably an aspartimide, was observed when using 3.0 equivalents of *tert*-butyl bromoacetate/DIEA according to the reported method<sup>43</sup> (Figure S4; Figure S8: LCMS indicating  $\Delta m/z$  of -32 compared to 8,  $>60\%$  of the total peak area; Scheme S2). Using 6.0 equivalents of base and alkylating agent minimized this side reaction to undetectable levels.

Subsequent basic hydrolysis of the methyl ester of 8 by suspension in a 1:1 mixture of THF/MeOH saturated with LiOH for 15 min was successful, yielding 9 on resin. Finally, 9 was fully deprotected and cleaved from the resin using a 95:5 mixture (v/v) TFA/  $\text{H}_2\text{O}$ , yielding the final product, NDL-1 or NLL-1. NDL-1 and NLL-1 were isolated by diethyl ether precipitation to form a fine white or off-white powder. The calculated yields were 64.2% and 90.3% for NDL-1 and NLL-1, respectively. The identities of NDL-1 and NLL-1 were confirmed by HRMS-TOF (ESI+): calculated for  $\text{C}_{20}\text{H}_{35}\text{N}_5\text{O}_9$   $[\text{M}+\text{H}]$  490.2508; found 490.2456 (NDL-1) and 490.2503 (NLL-1), respectively (Figure S5).

UV-LCMS analysis of NDL-1 revealed the presence of split peaks, both with  $m/z$  values corresponding to that of the desired product ( $m/z$  of 490.2, Figure S4). These peaks were successfully separated and purified using semi-preparative HPLC and designated as NDL-1 and NDL-2, achieving purities  $>98\%$ , as indicated by analytical HPLC (Figure 2). Similar results were obtained for NLL-1 (Figure S6).

### Differential characterization of NDL-1 and NDL-2

The compound peaks ascribed to NDL-1 and NDL-2 were initially believed to be diastereoisomers of NDL-1. However, subsequent radio-HPLC characterization and radiolabeling optimization attempts revealed that NDL-2 is most probably an epimerized  $\beta$ -aspartyl or  $\alpha$ -aspartyl rearranged by-product resulting from aspartimide by-product formation during the synthesis of (8) and its subsequent cleavage during the synthesis of (9). The chemical structures of the two compounds featured in Figure 2 and Scheme S2 showcase the products of the proposed intra-molecular rearrangement, which has been highlighted for clarity. This side reaction is well documented in SPPS-related literature and is further described in the context of NDL in Scheme S2.<sup>44, 45</sup>

This was further substantiated by radio-HPLC analysis of  $^{68}\text{Ga}$ -NDL-1 and  $^{68}\text{Ga}$ -NDL-2, which revealed slightly split radio-peaks for each radiolabeled compound (Figure S7A). If NDL-1 and NDL-2 were clearly separated diastereoisomers, a single radio-HPLC peak was to be expected. Additionally, significantly poorer  $^{68}\text{Ga}$ -chelation efficiency was observed for NDL-2 when compared to NDL-1 under identical radiolabeling conditions (Figure S7B). This is most likely due to the alteration of the NODASA core structure in NDL-2, which negatively affected its capability to efficiently chelate

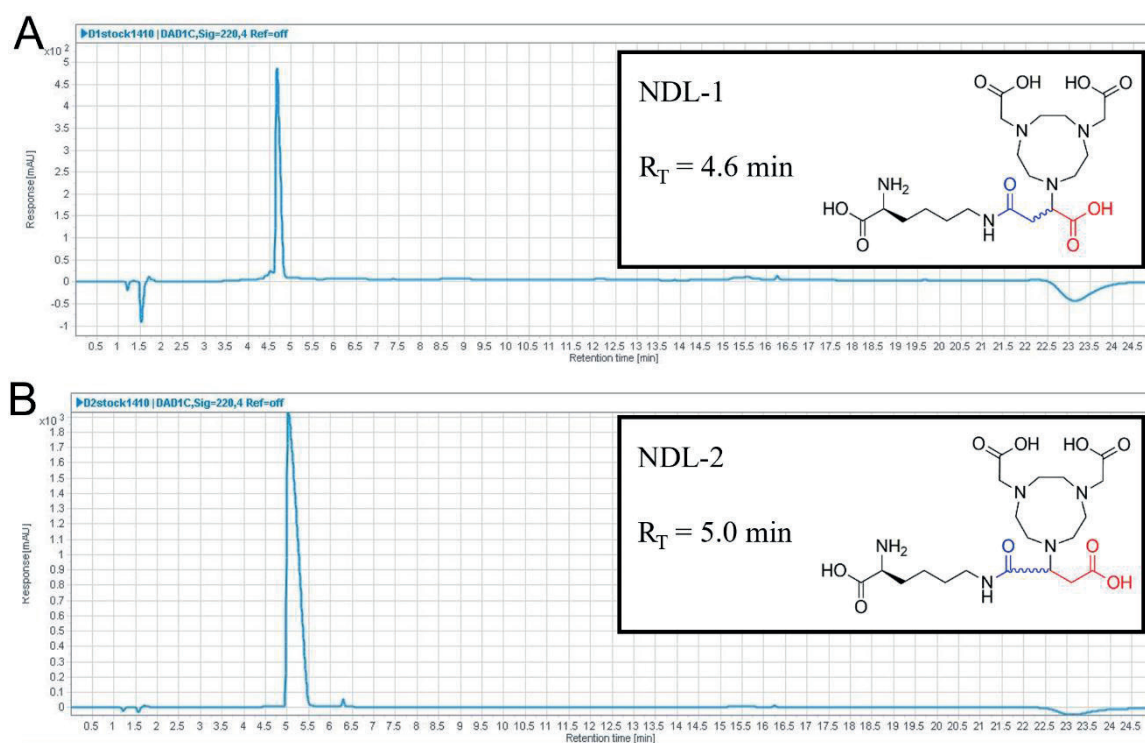


**Figure 2:** HPLC (UV 220 nm) analysis of purified (A): NDL-1 and (B): NDL-2 and their proposed chemical structures. Identical results were obtained for NLL-1 and NLL-2 (Figure S6).

gallium, since the structure is optimised to the ionic radius of  $\text{Ga}^{3+}$ . Lastly, the NDL-2 by-product yield at the end of synthesis correlated well with the increased aspartimide by-product formation observed during the synthesis of (8) (Figure S8). Similar results were obtained for NLL-1 and NLL-2 (data not shown). Thus, based on the evidence that indicates the formation of structural isomers during synthesis and poor  $^{68}\text{Ga}$ -chelation capability, isolated NDL-2 and NLL-2 products were excluded from further experimentation, and we proceeded with the desired NDL-1 and NLL-1 products.

#### Analytical characterization of $[^{68}\text{Ga}]\text{Ga}$ -NDL-1 and $[^{68}\text{Ga}]\text{Ga}$ -NLL-1

To assess whether NDL-1 and NLL-1 could successfully incorporate gallium-68, general radiolabeling was performed using a protocol adopted from Rossouw and Breeman,<sup>46</sup> followed by radio-HPLC analysis (method 1) of the resulting radiolabeled products. The results are shown in Figure 3. Both NDL-1 and NLL-1 successfully incorporated gallium, as indicated by the specific  $[^{68}\text{Ga}]\text{Ga}$ -NDL-1 and  $[^{68}\text{Ga}]\text{Ga}$ -NLL-1 peaks emerging at  $R_T = 2.7$  min (Figure 3A and 3B, respectively) which were separated from that of the free, ionic  $^{68}\text{Ga}$ -species ( $R_T = 1.65$  min, but 1.4 – 2.4 min broad, Figure S9). No UV signals corresponding to this peak were detected. This was expected, as NDL-1 and NLL-1 exhibit very limited UV absorbance. Furthermore, a marked difference in  $R_T$  was observed between NDL-1 and  $[^{68}\text{Ga}]\text{Ga}$ -NDL-1 ( $\Delta t = 4.7$  min) (Figure 3C). This is expected because of the altered physicochemical properties of NODASA upon radiometal chelation, which constitutes a large proportion of the overall molecular structure. While no additional radiopeaks were observed, the possibility of radiolabeled impurity co-elution due to the short retention time of the radioconjugate cannot be excluded. Thus, complementary UV-LCMS (UV 220 nm) analysis of a more concentrated non-radioactive reference compound (Ga-NDL-1) was performed to confirm the identity of  $[^{68}\text{Ga}]\text{Ga}$ -NDL-1 (Figure 3D). The  $R_T$  of Ga-NDL-1 (2.57 min, with a confirmed  $m/z$  of 556.2, Figure 3E) correlated well with the  $R_T$  of  $[^{68}\text{Ga}]\text{Ga}$ -NDL-1, confirming that the corresponding radioconjugate was indeed obtained in the labelling reactions. The small difference in  $R_T$  between the radiolabeled and

cold compounds was a result of the delay time between the instrument detectors. No additional peaks or  $m/z$  signals were observed (except for a confirmed unretained buffer-related peak at  $R_T = 2.0$  min), indicating that a chemically pure metal conjugate was obtained.

Radio-HPLC methods 1 and 2 were sufficient for monitoring the radiolabeling performance (baseline separation between ionic  $^{68}\text{Ga}$  and radiolabeled compounds) and radiometal-conjugate stability from a radiotracer development perspective. It should also be noted that the developed radio-HPLC method can separate  $[^{68}\text{Ga}]\text{Ga}$ -NDL-1 from excess unreacted NDL-1 ligand in a relatively short time, and thus may be adapted for preparative-HPLC purification. This would enable the production of a radiopharmaceutical product devoid of excess unreacted ligand that may compete with  $[^{68}\text{Ga}]\text{Ga}$ -NDL-1 for target-site binding in biological assays.<sup>47, 48</sup>

#### Development and evaluation of optimal radiolabeling parameters

Developing a new radiosynthesis method includes the evaluation of radiolabeling parameters that warrant reliable production of a radiolabeled product at low ligand concentration and in the shortest amount of time. A series of reactions was performed to assess the radiolabeling outcome based on the following variables: 1) ligand concentration (2.5, 5.0, 10, and 20  $\mu\text{M}$ ); 2) eluate acidity (pH 3.5 vs. pH 4.5); 3) reaction temperature (room temperature vs. 80°C); and 4) reaction time (5, 10, and 20 min). The experimental pH values were selected from NOTA-based gallium-68 radiolabeling literature, citing a pH between 3 – 5 to be essential<sup>41, 42</sup>. The results are presented in Table 2. Quantitative radiolabeling of both  $[^{68}\text{Ga}]\text{Ga}$ -NDL-1 and  $[^{68}\text{Ga}]\text{Ga}$ -NLL-1 were achieved at 80°C in as little as 10 min using a ligand concentration as low as 5  $\mu\text{M}$  with generator eluates adjusted to pH 4.5.

Remarkably poor radiochemical yields (RCY) were achieved at pH 3.5 when compared to those at pH 4.5. This is an unexpected result, as most reactive  $\text{Ga}^{3+}$  species, such as  $[\text{Ga}(\text{H}_2\text{O})_6]^{3+}$ , predominate in solutions below pH 4.0, which should facilitate an improved labelling efficiency.<sup>41, 42</sup> Indeed, NOTA-based chelators are known for their excellent chelating capacity at low pH (3.0–4.0).<sup>41</sup> Nonetheless, at



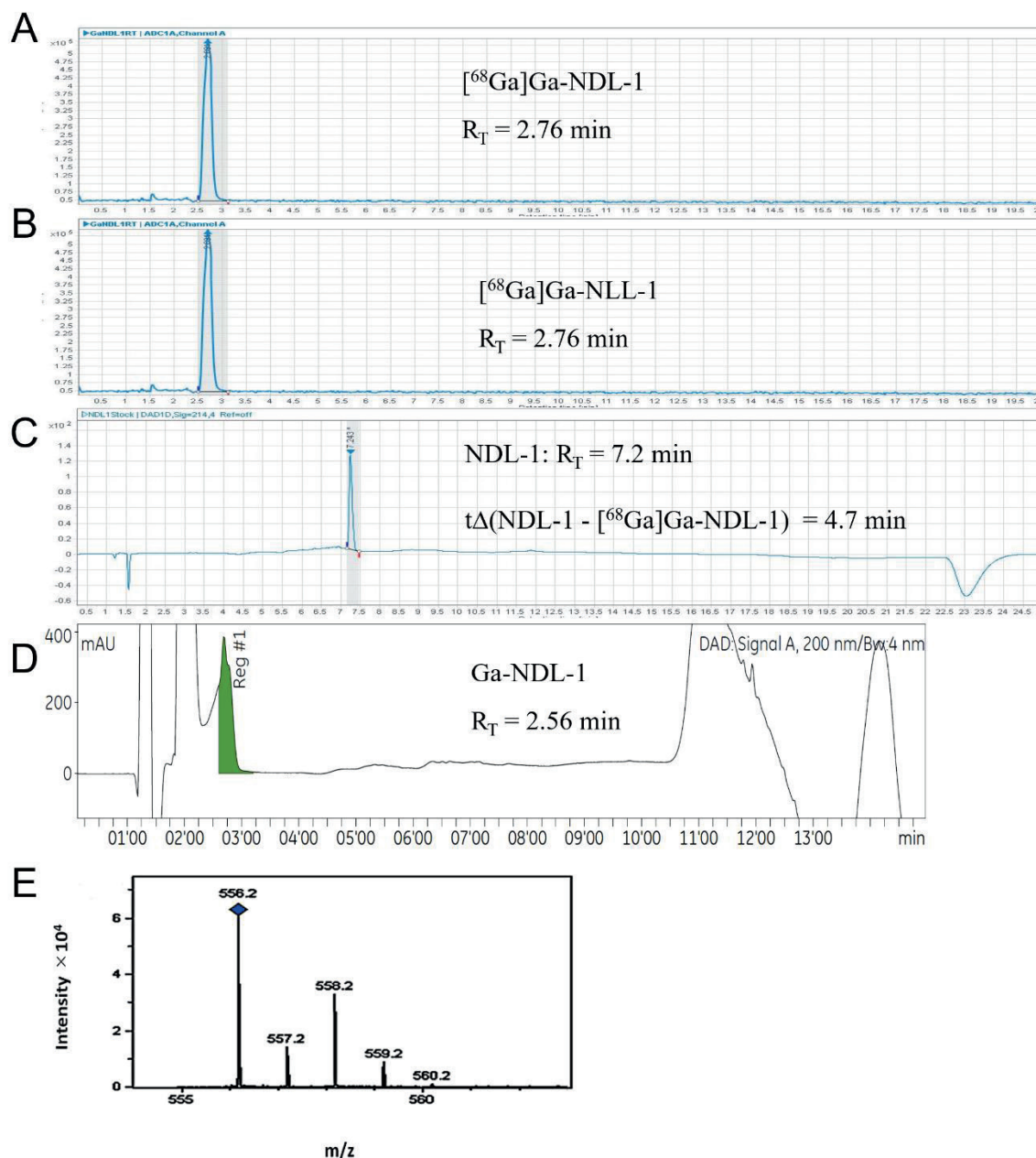


**Figure 3:** Radio-HPLC characterisation of  $[^{68}\text{Ga}]\text{Ga-NDL-1}$ . (A) Radio-chromatogram (cps) of  $[^{68}\text{Ga}]\text{Ga-NDL-1}$  and (B)  $[^{68}\text{Ga}]\text{Ga-NLL-1}$ ; (C) UV<sub>220 nm</sub> chromatogram of an NDL-1 stock solution (1 mg/mL) used for radiolabeling ( $R_T = 7.1\text{--}7.3$  min); (D) complementary UV<sub>220 nm</sub> chromatogram of 'cold' reference  $^{nat}\text{Ga-NDL-1}$  compound ( $R_T = 2.5\text{--}2.7$  min); (E) mass spectrum of non-radioactive Ga-NDL-1. Multiple signals ( $m/z$ ) are indicative for the isotopic distribution of  $^{nat}\text{Ga}$  which includes: 556.2 (100%), 558.2 (71%), 557.2 (24%), 559.2 (17%), 560.2 (3.1%).

pH 4.5, consistent and quantitative radiolabeling yields of  $[^{68}\text{Ga}]\text{Ga-NDL-1}$  and  $\text{NLL-1}$  were achieved at concentrations as little as  $5.0\ \mu\text{M}$  in less than 5 min when heated to  $80^\circ\text{C}$ . At this pH, quantitative labelling could also be achieved at room temperature, but with an increased incubation time of up to 20 min. being required. At NDL-1 concentrations  $\leq 5.0\ \mu\text{M}$ , increased temperature yielded higher %RCY compared to room temperature, though the yield plateaued within 5 min of reaction time. The same result was observed for NLL-1; however, a lower overall %RCY was achieved. This may be a result of inter-gallium eluate variability between the three sets of experiments in terms of activity and degree of metallic impurities. For example, significant amounts of  $\text{Zn}^{2+}$  are generated within the generator as  $^{68}\text{Ga}$  decays over time, thus its presence is more prominent in the first eluate of the day.<sup>42</sup> For NOTA-based chelators,  $\text{Zn}^{2+}$  is known to compete with  $^{68}\text{Ga}$  and adversely affects  $^{68}\text{Ga}$ -radiolabeling performance, especially at low added ligand concentrations.<sup>42, 47, 49, 50</sup>

It should be noted that for radiolabeling at pH  $> 4.0$ , precipitation of water-insoluble  $[^{68}\text{Ga}]\text{Ga}(\text{OH})_3$ -species (a.k.a. colloids) is a concern,

as this can result in a situation where the rate of gallium-chelate complex formation essentially competes with the rate of colloid formation.<sup>47</sup> The prevalence of such colloids cannot be quantified by HPLC, but could be assessed in later routine labelling experiments using solid phase extraction (SPE) to capture and measure excess colloids. Nonetheless, the observed loss of activity to SPE cartridges was consistently relatively low ( $< 10\%$ , refer to the next section).

It should also be noted that none of the samples showed any additional radiopeaks during radio-HPLC analysis. This indicates the absence of ligand impurities that may compete with NDL-1/NLL-1 for gallium-68 chelation, whether due to ligand degradation under labelling conditions (oxidation or radiolysis) or the presence of UV-inactive ligand by-products carried over from the chemical synthesis procedure. This also indicates that either the  $^{68}\text{Ga-NDL-1}$  or  $^{68}\text{Ga-NLL-1}$  complex is highly stable and resistant to thermolytic cleavage during the 20 min exposure to the high-temperature period (Figure 4). However, the possibility of degradation and by-product co-elution during HPLC analysis remains, as previously mentioned.

**Table 2:** Summarized results for  $^{68}\text{Ga}$ -radiosynthesis optimizations

Name	Eluate Acidity (pH)	Temperature (RT or °C)	Incubation Time (min)	Molarity (NDL-1/NLL-1) during radiosynthesis			
				2.5 μM	5 μM	10 μM	20 μM
Radiochemical purity (%)							
NDL-1	3.5	RT	05	0.12	19.69	41.47	-
NDL-1	3.5	RT	10	0.23	23.97	56.73	-
NDL-1	3.5	RT	20	0.29	24.16	58.06	-
NDL-1	3.5	80	05	2.28	5.26	26.45	97.70
NDL-1	3.5	80	10	3.00	6.39	34.01	98.57
NDL-1	3.5	80	20	6.15	12.87	52.26	98.33
NDL-1	4.5	RT	05	60.63	84.43	94.66	94.22
NDL-1	4.5	RT	10	69.21	89.82	97.79	97.51
NDL-1	4.5	RT	20	65.12	96.77	97.83	97.66
NDL-1	4.5	80	05	79.28	98.63	98.23	98.26
NDL-1	4.5	80	10	78.22	98.63	98.71	97.44
NDL-1	4.5	80	20	78.62	98.36	98.38	97.49
NLL-1	4.5	80	05	55.75	98.74	97.67	97.23
NLL-1	4.5	80	10	56.67	98.44	98.95	97.20
NLL-1	4.5	80	20	57.10	98.88	99.16	96.91

Footnotes: values in gray-highlighted area featuring best radiolabeling conditions (i.e., RCP>90%) whereas values within red-highlighted areas featuring undesired radiolabeling conditions (i.e., RCP<60%).

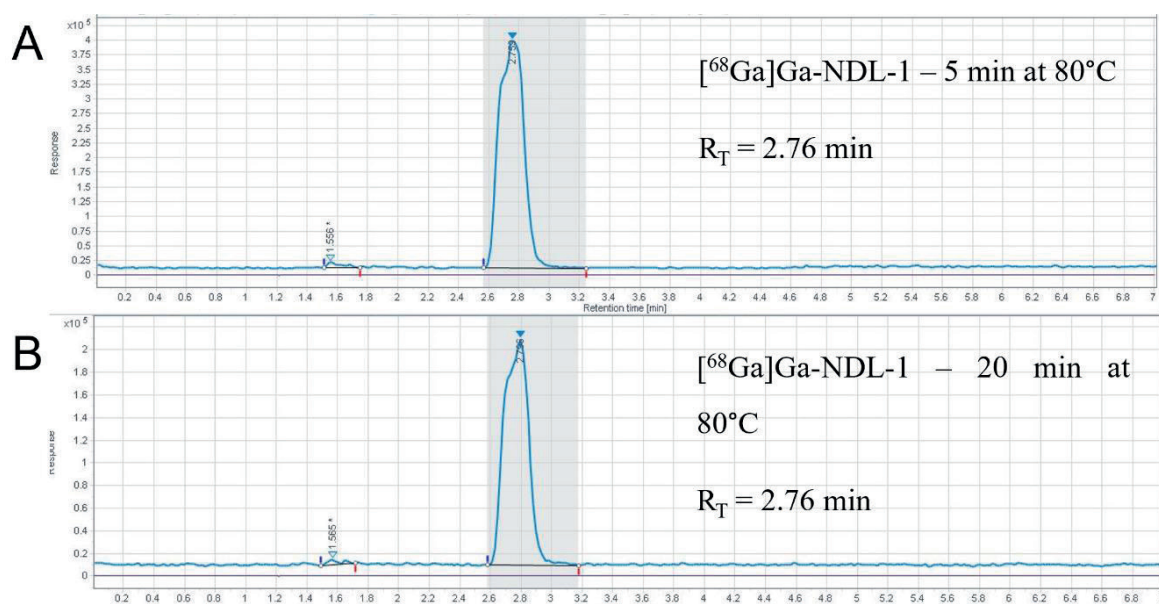


**Figure 4:** Radio-HPLC analysis of  $^{68}\text{Ga}$ -NDL-1 recorded after (A) 5 min and (B) 20 min of incubation at 80°C in the reaction solution, indicating sustained resistance to thermolytic cleavage.

### SPE purification method development

To obtain a radiolabeled product suitable for injection, insoluble  $^{68}\text{Ga}$ -colloids and excess reaction buffer salts must be removed from the radiolabeled products using SPE.<sup>40, 47</sup> However, an initial comparison of such SPE cartridges recommended for purification of  $^{68}\text{Ga}$ -radiolabeled products (i.e., Waters Sep-Pak C18 Light, Waters Sep-Pak CM (cation exchange)) failed to fully capture and retain  $^{68}\text{Ga}$ -NDL-1 or  $^{68}\text{Ga}$ -NLL-1 during sample loading and the initial wash phase (by using solvent systems recommended by the manufacturer).<sup>40, 47</sup> Therefore, an original SPE purification method was developed in this study.

The comparison of different SPE stationary phases revealed that Waters Sep-Pak Silica plus cartridges could efficiently retain the radio-conjugates if the reaction solution was diluted with 9-times excess

EtOH (i.e. solvent composition of 90% EtOH/water) and recovered with increasing water/PBS (PBS = phosphate-buffered saline) solvent composition. As the literature has not yet reported any protocols on silica-based SPE to purify  $^{68}\text{Ga}$ -radiolabeled products, we investigated several elution profiles to characterize target product and unreacted ionic- $^{68}\text{Ga}$ -species desorption and propose success rates for purification performance. **Table 3** lists the solvent composition of each elution fraction used as part of each elution profile. **Figure 5** provides a summary of the SPE desorption trends of  $^{68}\text{Ga}$ -NDL-1 activity.

For the purpose of de-salting (2.5M NaOAc was used) and removal of gallium-68 colloids, a 1-step recovery of major amounts of  $^{68}\text{Ga}$ -NDL-1 radioactivity from the cartridge was sufficient using water/PBS; however, unreacted, ionic- $^{68}\text{Ga}$ -species may also co-elute. As a solution, employing gradual elution profiles (e.g., profiles



**Table 3:** Solvent composition of each Waters Sep-Pak Silica plus SPE cartridge elution profile \*.

	Elution Fraction 1	Elution Fraction 2	Elution Fraction 3	Elution Fraction 4	Elution Fraction 5
Elution Profile 1	1.0 mL PBS				
Elution Profile 2	2.0 mL H <sub>2</sub> O				
Elution Profile 3	2.0 mL 60% EtOH/ H <sub>2</sub> O	2.0 mL 40% EtOH/ H <sub>2</sub> O	2.0 mL H <sub>2</sub> O		
Elution Profile 4	1.0 mL 70% EtOH/ H <sub>2</sub> O	1.0 mL 50% EtOH/ H <sub>2</sub> O	0.5 mL 50% EtOH/H <sub>2</sub> O	0.5 mL 50% EtOH/ H <sub>2</sub> O	
Elution Profile 5	1.0 mL 90% EtOH/ H <sub>2</sub> O	1.0 mL 80% EtOH/ H <sub>2</sub> O	1.0 mL 70% EtOH/ H <sub>2</sub> O	1.0 mL 60% EtOH/ H <sub>2</sub> O	1.0 mL 50% EtOH/ H <sub>2</sub> O

Footnotes: \*) elution profiles 1-5 all contained a wash/rinse step with 2.0 mL 90% EtOH/H<sub>2</sub>O prior to elution.

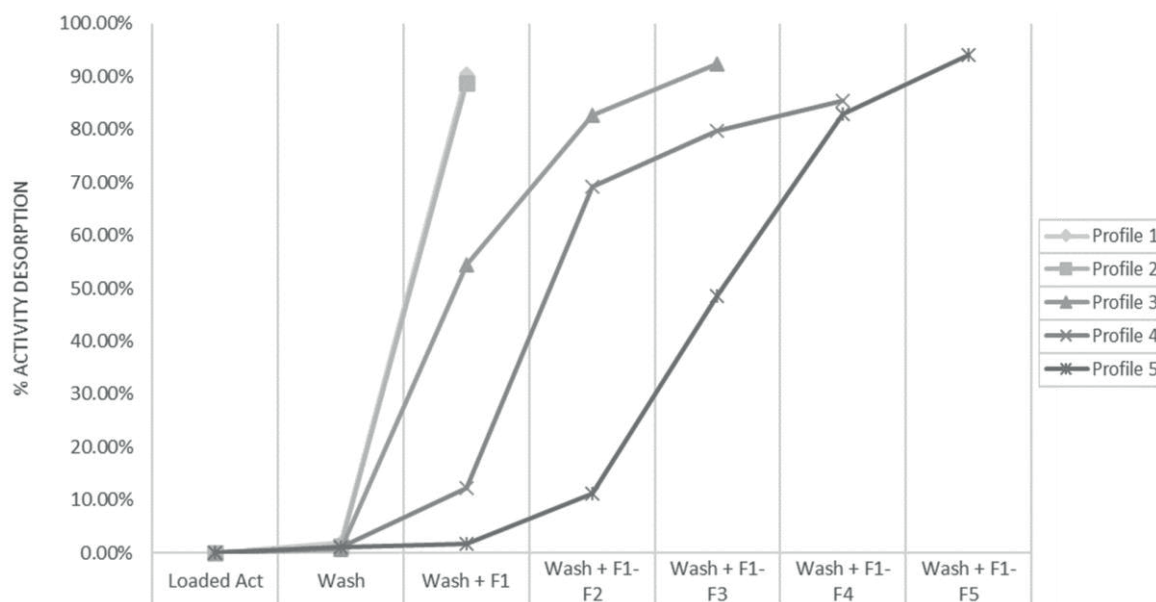


**Figure 5:** Summary of the [<sup>68</sup>Ga]Ga-NDL-1 activity recovery from Waters Sep-Pak Silica plus SPE cartridges using five different elution profiles. The elution profiles are listed in **Table 3**.

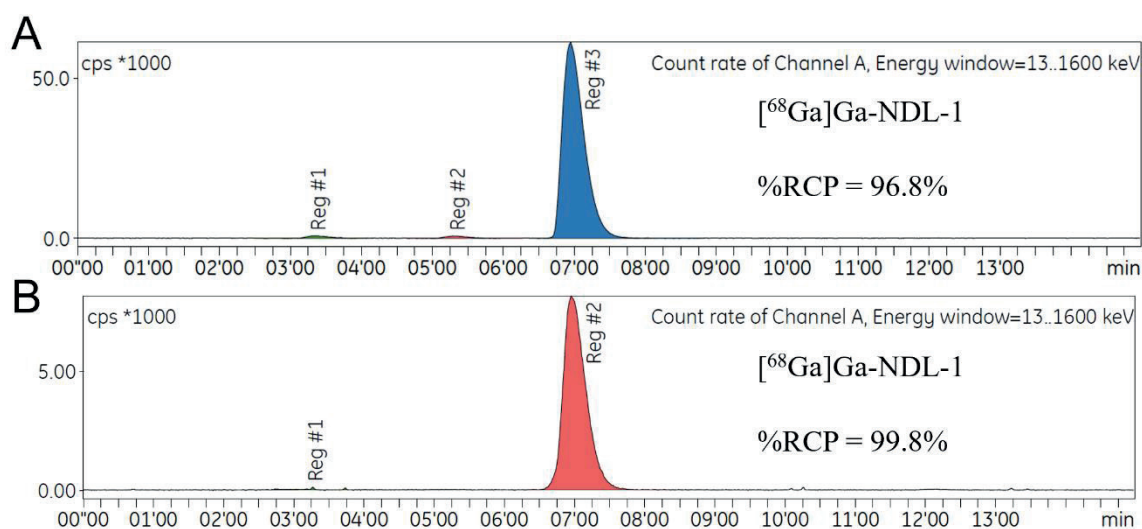


**Figure 6:** Radio-HPLC analysis (method 2) of Waters Sep-Pak Silica plus SPE elution profile 3: F1 (A) and F2 and F3 combined (B), indicating successful removal of unreacted, ionic <sup>68</sup>Ga.

3-5) provided pure fractions devoid of ionic-<sup>68</sup>Ga, thereby affording radiochemical purity (RCP) >99.8% from 97.2% crude (for example: Profile 3: F1 = 97.2%; F2/3 = >99.8%, **Figure 6**), but at the expense of the overall RCY. A minimum of 80% EtOH/water (20% water) was required to recover activity from the cartridge.

As mentioned, for radiolabeling at pH >4.0, precipitation of <sup>68</sup>Ga-colloids is a concern.<sup>47</sup> SPE is a well-accepted method used to capture and remove chemically inert and insoluble <sup>68</sup>Ga-colloids from the final product.<sup>42</sup> Fortunately, we found that the apparent loss of radioactivity

to the SPE (including colloids) at the end of purification remained relatively low for all SPE settings investigated ( $9.7 \pm 2.8\%$ ,  $n = 8$ ).

It should be noted that, interestingly, use of silica-based SPE purification of <sup>68</sup>Ga-radiopharmaceuticals has not been reported in literature. In fact, limited information is available on the mechanism in which the sorbent material of commonly used SPE cartridge-types is involved (whether it be due to a filtering effect, or chemical affinity).<sup>47-49, 51-54</sup> Thus, to confirm that silica-SPE also has the capacity to capture and remove <sup>68</sup>Ga-colloids, a control experiment was

performed on a sample containing predominantly colloidal- $^{68}\text{Ga}$  species. The sample's  $^{68}\text{Ga}$ -colloid content was quantified using an iTLC-SG (silica gel) method: 0.1 M sodium citrate (pH 5) as mobile phase to separate  $^{68}\text{Ga}$ -colloidal species ( $R_f = 0.1$ ) from free ionic- $^{68}\text{Ga}^{3+}$  that migrate with the solvent front ( $R_f = 0.8$ ).<sup>53</sup> This control experiment demonstrated that silica-SPE also captures and removes chemically inert and insoluble  $^{68}\text{Ga}$ -colloids, as after cartridge loading, no desorption occurs irrespective of eluting solvent strength applied. Therefore, the proposed SPE protocol is suitable for providing radiochemically pure [ $^{68}\text{Ga}$ ]Ga-NDL-1 and [ $^{68}\text{Ga}$ ]Ga-NLL-1 as starting materials for different characterisation assays (and future administration to live species).

Nonetheless, as a potential alternative to SPE, the developed radio-HPLC methods could also sufficiently separate [ $^{68}\text{Ga}$ ]Ga-NDL-1/NLL-1 from excess unreacted ligand (Figure 3) in a relatively short run-time. Thus, these methods may also be adapted to isolate [ $^{68}\text{Ga}$ ]Ga-NDL-1 from excess NDL-1 (which may compete with the mechanisms governing enzymatic incorporation of D-AA into PG in biological assays).<sup>47, 48</sup>

### Optimized radiosynthesis protocol performance

Based on results from the evaluated radiolabeling and SPE parameters, the following radiosynthesis protocol has been adopted for routine radiolabeling: a ligand concentration of 5  $\mu\text{M}$  in buffered  $^{68}\text{Ga}$ -eluate (pH set at 4.0–4.5) is incubated at 80°C for 10 minutes. To remove excess buffer salts and colloidal- $^{68}\text{Ga}^{3+}$ , the radiolabeled product is subsequently cleaned with a Water's Sep-Pak Silica SPE using either 2.0 ml water or 2.0 mL PBS as desorption agent.

Key radiolabeling performance parameters such as %RCY, %RCP, product activity at the end of synthesis (E.O.S), and apparent molar activity ( $A_m$ ) was calculated by repeated radiosyntheses with the inclusion of SPE purification. Table 4 provides a summary of the results gathered from consecutive preparations of [ $^{68}\text{Ga}$ ]Ga-NDL-1 and -NLL-1 using this novel radiosynthesis protocol. Data were pooled based on identical physicochemical properties and similar radiolabeling parameters. In comparison, results from several radiolabeling reactions performed at lower NDL-1 / NLL-1 concentrations (2.5 $\mu\text{M}$  and 1.0 $\mu\text{M}$ ) are also provided.

Reliable radiolabeling was achieved with the proposed protocol, indicating the successful, high-quality preparation of a radiochemically pure product (%RCP >95%). Relatively high levels of %RCY and  $A_m$  were consistently achieved in under 60 minutes of total radiosynthesis time. By using silica SPE, radiochemically pure products that are suitable for further *in vitro* and *in vivo* application-based experimental assays can be produced with molar activities ( $A_m$ ) similar to other reported  $^{68}\text{Ga}$ -radiolabeled NOTA-based chelator-functionalised peptides, such as [ $^{68}\text{Ga}$ ]Ga-NOTA-UBI (13.8  $\pm$  1.9 GBq/ $\mu\text{mol}$ ),<sup>55</sup> [ $^{68}\text{Ga}$ ]Ga-NOTA-RGD-GE11 (>35.2 GBq/ $\mu\text{mol}$ ),<sup>56</sup> and NODAGA-functionalized peptide heterodimer derivatives (25–61 GBq/ $\mu\text{mol}$ ).<sup>57</sup>

It should be noted that the relatively lengthy radiosynthesis time caused substantial decay-related loss in product  $A_m$ . However, the total radiosynthesis can be substantially reduced by applying a faster loading/elution flowrate,<sup>58</sup> an automated radiosynthesis modality that exclude operator-related limitations,<sup>51</sup> or through pre-concentration of  $^{68}\text{Ga}$ -eluate before radiosynthesis to allow for smaller reaction volumes.<sup>49</sup> For example, the bulk of added radiosynthesis time could be attributed to SPE purification (37.1  $\pm$  3.8 min), where almost a half (17.0  $\pm$  2.5 min) could be attributed to loading the cartridge with the ethanol-diluted crude product at a low flowrate (10.0 mL at 0.5 – 0.8 mL/min). By reducing the radiolabeling reaction volume, or applying a faster and more consistent loading/elution flowrate (e.g. between 1 – 5 mL/min as commonly reported in literature), the total radiosynthesis time could be majorly reduced.<sup>58</sup>

An added benefit of using the herein developed silica-based SPE together with water or PBS as stronger desorption solvent may be a possible production of a radiotracer product ready for injection

**Table 4:** Result summary from upscaled radiosyntheses for [ $^{68}\text{Ga}$ ]Ga-NDL-1 and [ $^{68}\text{Ga}$ ]Ga-NLL-1 preparation (pooled data\*)

Total number of radiosyntheses	26
Generator elution technique	Eluate fractionation (EF)
$^{68}\text{Ga}$ -activity yield (2.0 mL EF fraction) (MBq)	709 $\pm$ 115
$^{68}\text{Ga}$ -waste fraction (%)	8.1 $\pm$ 3.3
Buffer solution for eluate acidity adjustment	2.5M Sodium Acetate
Buffered eluate acidity measured (pH value)	4.5 $\pm$ 0.5
Optimal reaction temperature (°C)	80
Reaction time (min)	10
Radiolabeling reproducibility	
Scaled to 1.0 mL EF activity reactions: (n)	18
Added radioactivity (MBq)	201 $\pm$ 23
5.0 $\mu\text{M}$ NDL/L: (n)	10
RCY $\geq$ 95%: n (%)	10 ( <b>100</b> )
RCY (%)	97.3 $\pm$ 0.2
2.5 $\mu\text{M}$ NDL/L: (n)	6
RCY $\geq$ 90%: n (%)	4 ( <b>67</b> )
RCY (%)	95.7 $\pm$ 2.6
1.0 $\mu\text{M}$ NDL/L: (n)	2
RCY $\geq$ 90%: n, (%)	0 (0)
RCY (%)	27.0 $\pm$ 19.9
Scaled to 0.5 mL EF activity reactions: (n)	8
Added radioactivity (MBq)	106 $\pm$ 31
5.0 $\mu\text{M}$ NDL/L: (n)	8
RCY $\geq$ 90%: n, (%)	7 ( <b>88</b> )
RCY (%)	98.3 $\pm$ 0.9
Robustness SPE purifications (n)	6
Radio-HPLC method used	Method 2 (see Table 1)
SPE cartridge type	Sep-Pak Silica plus
Sample volume (mL)	10.0
Sample composition	EtOH/reaction solution (9:1 v/v)
Product elution agent (mL)	Water or PBS (1.8 – 2.1)
Desorption rate (%)	85.3 $\pm$ 2.8
Crude RCY (%)	97.3 $\pm$ 0.4
Post-Purification RCY (%) <sub>decay-corrected</sub>	81.7 $\pm$ 3.2
Post-Purification RCP (%)	97.7 $\pm$ 0.5
$A_m$ (E.O.S; GBq/ $\mu\text{mol}$ )	17.1 $\pm$ 0.8
Loss to apparatus / materials (%)	18.3 $\pm$ 1.6
Radioactivity cartridge matrix (colloids) (%)	9.1 $\pm$ 2.2
Preparation time (min)	37.0 $\pm$ 7.0
Recovered radioactivity (%)	99.0 $\pm$ 1.5

Footnotes: \*) results from repeated radiosyntheses are expressed as mean  $\pm$  SD (n $\geq$ 3) (if not stated otherwise).

without the need of EtOH evaporation (a lengthy step required when utilizing C18- or Hydrophilic-Lipophilic Balanced (HLB)-SPE) or dilution.<sup>47</sup> Injection of a radiopharmaceutical with high ethanol content may cause side effects such as pain and hemolysis, thus radiopharmaceutical solutions are generally limited to only 10% (v/v) ethanol.<sup>59</sup> EtOH evaporation also increases the risk of radioactive contamination and radiation exposure to operators, and may be accompanied by partial decomposition of the tracer via radiolysis.<sup>47</sup>

<sup>60</sup> In our developed silica-based SPE method, maximum desorption

was achieved with 100% water or PBS, thus eliminating the need for ethanol in radiolabeled-product preparation for injection.

One of the limitations of the silica-based SPE method is its reliance on the crude product RCP being of acceptable quality, i.e., it is often referred to “instant” radiolabeling ( $\geq 95\%$  RCY), as this method was not fully able to eliminate ionic  $^{68}\text{Ga}$ -species. As demonstrated, ionic  $^{68}\text{Ga}$ -species are also retained on the silica-SPE cartridge and can only be separated from  $^{68}\text{Ga}$ -NDL-1/NLL-1 by applying a gradual elution profile of increasing water strength. Although separation is achievable, it is at the sacrifice of some RCY due to a degree of overlapping elution.

It should be noted that the lack of reported use of silica-based SPE may be due to the retention of free ionic- $^{68}\text{Ga}^{3+}$ , as well as the fact that larger molecular scaffolds are typically used in  $^{68}\text{Ga}$ -radiochemistry due to the requirement of bifunctional metal-chelator functionalization for metal-based radionuclide incorporation. As a result, reverse-phase and ion exchange resins have been sufficient for separating  $^{68}\text{Ga}$ -radiolabeled compounds in general.<sup>48</sup> An additional concern is the incomplete removal of ionic germanium-68 from the final product using silica-based SPE, but this can be avoided by including pre-purification/concentration as part of the  $^{68}\text{Ga}$ -production process before radiolabeling application, such as ion-exchange chromatography, extraction chromatography, solvent extraction, precipitation, and electrochemical methods.<sup>51</sup> Nonetheless, due to the limited reported use of silica-based SPE purification of gallium-68 radiopharmaceuticals in literature, and its potential benefits as an alternative SPE for concentrating/purification of highly polar and hydrophilic compounds as demonstrated in this study, further investigations are warranted to characterize the capture and desorption behaviour of free ionic  $^{68}\text{Ga}$  species and generator-produced metal-contaminants.

Finally, it was demonstrated that quantitative labelling yields ( $>90\%$  RCY) could also be achieved with  $2.5\ \mu\text{M}$  NDL-1 to further increase the  $A_m$ ; however, due to variability, more comprehensive testing should be performed to support the preliminary results. This may include using more standardized production of  $^{68}\text{Ga}$ -activity by using a newer generator, or by means of activity concentration and pre-purification that limits metal contaminants as this could directly affect the radiolabeling efficiency.<sup>51–53</sup>

## Challenge and stability studies

Developing an original radiosynthesis protocol for a new compound, such as NDL, is commonly followed by a feasibility study that will cover the challenges for its general intended use, that is, radiopharmaceutical product integrity. Therefore, essential and often considered a go vs. no-go criterion, the concern of radiochemical product stability defines the time period in which the new  $^{68}\text{Ga}$ -NDL-1 or  $^{68}\text{Ga}$ -NLL-1 can be safely used for the intended purpose (e.g., integrity post-labelling until patient administration occurs). Results displayed in **Table 5** show a maintained  $^{68}\text{Ga}$ -chelation when challenged for up to 180 min and by using quantitative radio-HPLC analysis (at bench-top condition, PBS formulation; **Figure S10**). No apparent reduction in the % intact radioconjugate as well as visible re-occurrence of uncomplexed  $^{68}\text{Ga}$ -species or other by-product radio-peaks were observed. Percentage intact radioconjugate values higher than 100% were attained, most likely because of continuous chelation occurring

over time. These results, in combination with maintained quantitative radiolabeling being achieved and maintained for more than 20 minutes at  $80^\circ\text{C}$ , indicates a high level of thermodynamic stability.<sup>61</sup>

Another key criterion is that once the radiometal-chelator (NODASA) complex is formed, it should remain stable or irreversible, even in the presence of competitive chelating agents (mimicking biologically occurring metal scavengers).<sup>61</sup> If radiometals such as  $\text{Ga-68}$  are significantly released once injected into living species, it may result in non-specific biodistribution, off-target pharmacology, or compromised PET image quality.<sup>13</sup> Thus, to assess the kinetic inertness of the radioconjugate, a trans-chelation challenge using up to 1000-fold molar excess of EDTA is considered a powerful way to test efficient gallium-chelation.<sup>62</sup> The results of quantitative HPLC radio-peak analysis are also displayed in **Table 5**. Only a 6–7% reduction in the amount of intact radioconjugate for both  $^{68}\text{Ga}$ -NDL-1 and NLL-1 were observed due to exposure to EDTA over 180 min. This is reasonable proof that NDL-1 and NLL-1 (by way of NODASA) form excellent, stable complexes with gallium-68, and radioisotope release (or leeching) is negligible to minimal over an appropriate duration or once administered *in vivo*, which are all sought-after properties of NOTA-based chelators (**Figure S11**).

## Physico-chemical characterization and proteolytic stability

Key properties such as lipophilicity, polar surface area, and net charge play pivotal roles in influencing the radiotracer's ability to permeate the blood–brain barrier or otherwise be delivered to tissues that may harbour active infection.<sup>63–65</sup> For instance, information gathered from numerous pharmacokinetic studies involving radiolabeled antibiotics underscores that delivery to body sites that show bacterial tissue manifestation can frequently be limited, primarily due to factors such as poor vascularisation, the presence of necrotic tissue, and elevated cellular density.<sup>4, 66</sup> Additionally, elevated plasma protein binding is often observed for highly lipophilic, small molecules, resulting in unfavourably slow clearance rates, while positively charged and hydrophilic radiotracers may be eliminated too swiftly. Thus, the degree of compound lipophilicity and binding to blood cells and plasma proteins are good predictors of its bioavailability and help enable (or may discourage) clinical translation.<sup>67</sup>

Herein, radio-conjugate blood cell association, serum protein binding and  $\text{LogD}_{7.4}$  (lipophilicity) were quantified to identify the blood residence time and test proteolytic stability. Both radio-conjugates showed low levels of blood cell and serum protein binding (**Figure 7**), which is a promising feature allowing for the prediction of potential *in vivo* behaviour following intravenous injection of  $^{68}\text{Ga}$ -NDL-1 or  $^{68}\text{Ga}$ -NLL-1. These results are in line with the low lipophilicity observed for both radio-conjugates ( $\text{LogD}_{7.4} = -2.78 \pm 0.12$  and  $-2.78 \pm 0.06$ , respectively). While the low blood-content binding is encouraging, the  $\text{LogD}_{7.4}$  value indicates that these compounds are extremely hydrophilic, which may restrict penetration of the hydrophobic bacterial outer-membrane (OM) in order to reach the target bacterial PG, prevent access to intracellular pathogens through lack of cell-wall penetration, or prevent sufficient interaction/binding with the target penicillin binding proteins (PBP) or transpeptidase proteins responsible for D-AA incorporation due to its polar surface area. Membrane-transport, however, may still be possible owing to the low molecular weight (MW) of the NDL-1/NLL-1 compounds. For instance, the outer membrane of gram-negative bacteria contains porins that allows import of water-soluble materials with a reported MW cargo-cutoff size of  $\sim 600\ \text{g/mol}$ , larger than the MW of radiolabeled and unlabelled NDL-1/NLL-1.<sup>31, 68</sup>

Interestingly, for  $^{68}\text{Ga}$ -NLL-1, a significant increase in blood cell association was observed after 60 min ( $P < 0.05$ ). In terms of serum protein binding, a significant decrease was observed at 60 min for both radioconjugates ( $P < 0.05$ ). However, a significantly larger decrease was observed for  $^{68}\text{Ga}$ -NLL-1 within 30 min compared

**Table 5:** Result summary on radiochemical stability for  $^{68}\text{Ga}$ -NDL-1 and  $^{68}\text{Ga}$ -NLL-1 from radio-HPLC analysis

Radiochemical stability	$^{68}\text{Ga}$ -NDL-1	$^{68}\text{Ga}$ -NLL-1
Bench-top ( $T_{180}$ )	100.9%	100.1%
PBS; pH 7.4 ( $T_{30}/T_{180}$ ) <sup>†</sup>	98.9% / 99.0%	100.5% / 100.5%
1000-fold excess EDTA ( $T_{30}/T_{180}$ ) <sup>†</sup>	98.0% / 94.3%	97.8% / 93.4%

Footnotes: <sup>†</sup> samples incubated at  $37^\circ\text{C}$ .



to its D-stereoisomer. Thus, it is plausible that some form of molecular interaction specific to L-amino acids may contribute to the observed differences in binding.

Since radiotracers are designed with high target specificity, it is important that the radiotracer remains stable in blood circulation until it reaches the target. If a radiotracer is not stable in blood plasma due to premature degradation or metabolism, the resulting fragments may exhibit altered biodistribution and non-specific off-target binding which can compromise PET image quality. Thus, the blood plasma enzymatic stability of [ $^{68}\text{Ga}$ ]Ga-NDL-1 and [ $^{68}\text{Ga}$ ]Ga-NLL-1 were tested for up to 120 min to determine their clinical translation potential.<sup>13</sup>

Both compounds remained stable throughout the duration of the challenge, with no emergence of free  $^{68}\text{Ga}$ -species or  $^{68}\text{Ga}$ -labeled by-products being observed. The results are displayed in **Table 6**, and comparative examples of the radio-chromatogram results for both radio-conjugates between  $T_0$  and  $T_{120}$  are displayed in **Figure 8**. It should be noted that, owing to the inherent limitations of our radio-HPLC method, the possibility of co-eluting degradation by-products cannot be

excluded. It should also be noted that degradation of the radio-conjugate may lead to the release of  $^{68}\text{Ga}$ , followed by sequestration by blood contents through either trans-chelation or electrostatic interaction between plasma proteins and degradation by-products through co-

**Table 6:** Results on proteolytic plasma stability for [ $^{68}\text{Ga}$ ]Ga-NDL-1/ -NLL-1 using radio-HPLC analysis

Serum stability*	[ $^{68}\text{Ga}$ ]Ga-NDL-1 (RCP%)		[ $^{68}\text{Ga}$ ]Ga-NLL-1 (RCP%)	
	Rep 1	Rep 2	Rep 1	Rep 2
$T_0$	n.d.	98.9	100.4	98.9
$T_{30}$	97.2	101.2	98.6	98.6
$T_{60}$	99.4	97.6	98.0	98.4
$T_{120}$	97.1	96.6	98.2	99.4

Footnotes: \*) normalised; n.d.) not determined; T) timepoint for sample preparation and analysis (0-120 min); Rep) individually repeated experiment (details see method section)

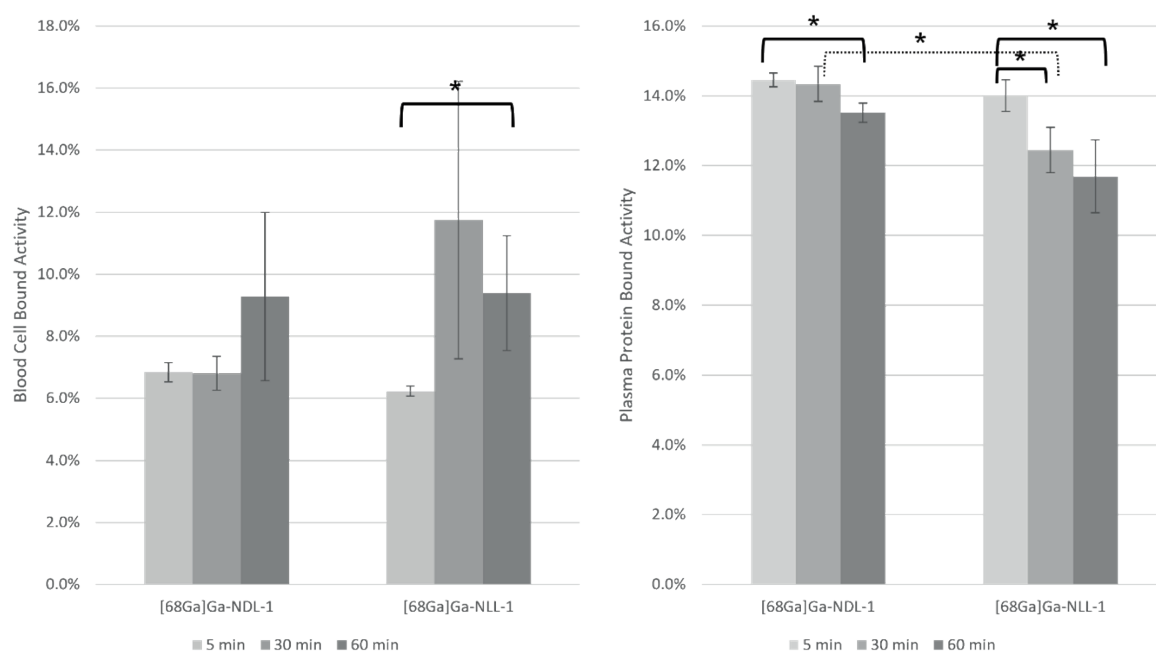


**Figure 7:** Percentile fraction of [ $^{68}\text{Ga}$ ]Ga-NDL-1 and [ $^{68}\text{Ga}$ ]Ga-NLL-1 associated with whole-blood cells (**left**) and plasma protein binding (**right**) following up to 60 min incubation at 37°C measured by automated gamma counting. Results are expressed as mean %Bound/Total activity  $\pm$  SD (n=3). A one-tailed paired student test comparing different time points of the same radiotracer (solid half-bracket) returned (\*)  $P < 0.05$ , and a two-tailed paired student test comparing [ $^{68}\text{Ga}$ ]Ga-NDL-1 and [ $^{68}\text{Ga}$ ]Ga-NLL-1 time points (dashed half-bracket) returned (\*)  $P < 0.05$ .

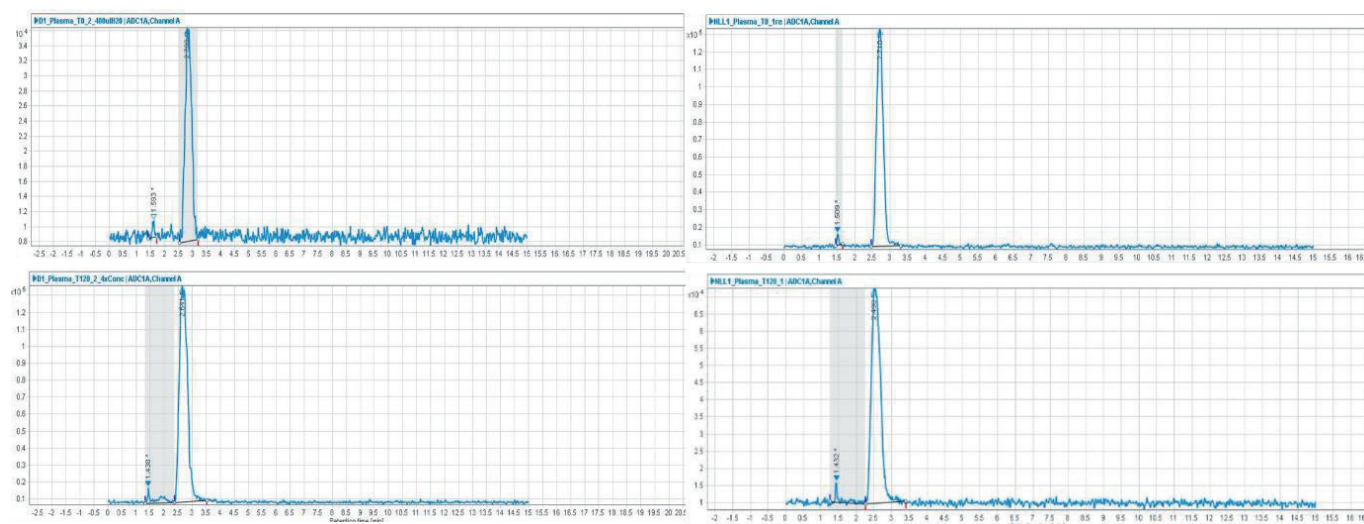


**Figure 8:** Plasma stability radio-chromatograms of [ $^{68}\text{Ga}$ ]Ga-NDL-1 (**left**) and [ $^{68}\text{Ga}$ ]Ga-NLL-1 (**right**) obtained at  $T_0$  (top) and  $T_{120}$  (bottom).

precipitation with EtOH during sample preparation. However, this scenario seems highly unlikely because the quantified percentage of protein-bound radio-conjugates significantly decreased over time for both [ $^{68}\text{Ga}$ ]Ga-NDL-1 and [ $^{68}\text{Ga}$ ]Ga-NLL-1 (Figure 8). This aspect is important, as the research scope for future studies is to evaluate whether [ $^{68}\text{Ga}$ ]Ga-NDL-1 is a bacteria-selective imaging agent. In contrast, [ $^{68}\text{Ga}$ ]Ga-NLL-1 is utilised as the negative control to demonstrate unwanted distribution and unspecific accumulation in bacteria based on the knowledge of the compound selectivity and specificity of PG biosynthesis, turnover, and remodelling.<sup>26, 31, 69</sup>

## CONCLUSION

To summarize, conjugation of small molecules with a metal-chelator to facilitate  $^{68}\text{Ga}$ -radiolabeling is still a relatively unexplored concept due to the obvious change the relatively bulky chelator imparts.<sup>61, 70</sup> However, the unselective nature of D-AA utilization and incorporation into bacterial PG, even when functionalised with relatively bulky fluorophores, provides a unique opportunity to explore  $^{68}\text{Ga}$ -radiolabeling of a single amino acid.<sup>31</sup> Thus, we developed a chemical synthesis for NODASA-functionalised D-lysine/L-lysine derivatives, and tested  $^{68}\text{Ga}$  chelation to form a radiolabeled product stable enough for further assessment as novel bacterial-specific radiopharmaceutical. The radiolabeling strategy was thus tested and optimized to achieve high RCY ( $81.7 \pm 3.2\%$ ) and  $A_m$  ( $17.1 \pm 0.8 \text{ GBq}/\mu\text{mol}$ ).

Our research shows that radiolabeling small, hydrophilic molecules using gallium radiochemistry methods poses its own challenges when it comes to purifying the resulting radiolabeled compounds. We highlighted that silica-SPE may prove useful in  $^{68}\text{Ga}$ -radiochemistry as an alternative to reverse-phase and ion-exchange resins by showing that separation of [ $^{68}\text{Ga}$ ]Ga-NDL-1/NLL-1 from colloidal- $^{68}\text{Ga}$ -species and unreacted ionic  $^{68}\text{Ga}$ -species is possible. However, further investigation is warranted to characterize the capture and desorption behaviour of free, ionic  $^{68}\text{Ga}$  species and generator-produced metal-contaminants, as according to our knowledge, no literature on this topic is available.

Through preliminary assays, we demonstrate that the [ $^{68}\text{Ga}$ ]Ga-NDL-1/NLL-1 compounds possess favorable physiochemical properties, such as high thermodynamic stability, kinetic inertness, proteolytic stability, and minimal blood content binding. These properties support future evaluation of [ $^{68}\text{Ga}$ ]Ga-NDL-1 as a bacterial-specific PET imaging agent, which will be assessed through *in vitro* bacteria cell uptake studies and small animal PET imaging studies.

## SUPPLEMENTARY INFORMATION

The radio-HPLC, ITLC and LCMS data of synthesized radiotracer precursors and crude radiolabeled products are available in the supporting information.

## ACKNOWLEDGEMENTS

The authors would like to thank the National Research Foundation (NRF) of South Africa, Catalysis and Peptide Research Unit (CPRU), College of Health Sciences (CHS), University of KwaZulu-Natal, The South African Nuclear Energy Corporation (Necsa), Nuclear Medicine Research Infrastructure (NuMeRI, NPC), Pre-clinical Imaging Facility (PCIF) staff, and Steve Biko Academic Hospital, Department of Nuclear Medicine, University of Pretoria.

## AUTHOR CONTRIBUTIONS

CAG: Conceptualization, Methodology, Synthesis, Radiolabeling, Stability Testing, Data Analysis, Writing – Original Draft; TN: Methodology, Writing – Review & Editing, Supervision, Funding Acquisition; JD: Radiolabeling, Stability Testing, Data Analysis; BGT: Methodology, Synthesis, Data Analysis; FA: Methodology, Synthesis, Data Analysis; HGK: Supervision, Funding Acquisition,

Writing – Review & Editing; BMP: Radiolabeling, Data Analysis; SM: Radiolabeling, Data Analysis; JRZ: Writing – Review & Editing, Supervision, Funding Acquisition; TE: Methodology, Writing – Review & Editing, Supervision, Funding Acquisition; TG: Conceptualization, Methodology, Writing – Review & Editing, Supervision, Funding Acquisition.

## DECLARATION OF COMPETING AND FINANCIAL INTERESTS

The authors declare that there are no competing interests.

## DECLARATION OF GENERATIVE AI AND AI-ASSISTED TECHNOLOGIES

The authors declare the use of Google Copilot to assists with language and text editing.

## ORCID ID

Christiaan A. Gouws: <https://orcid.org/0000-0002-9848-719X>  
 Tricia Naicker: <https://orcid.org/0000-0002-7134-6258>  
 Janie Duvenhage: <https://orcid.org/0000-0002-5770-7213>  
 Beatriz G. de la Torre: <https://orcid.org/0000-0001-8521-9172>  
 Fernando Albericio: <https://orcid.org/0000-0002-8946-0462>  
 Hendrik G. Kruger: <https://orcid.org/0000-0003-0606-2053>  
 Biljana Marjanovic-Painter: <https://orcid.org/0000-0001-8623-7321>  
 Sipho Mdanda: <https://orcid.org/0000-0003-0146-0538>  
 Jan Rijn Zeevaart: <https://orcid.org/0000-0003-0794-3012>  
 Thomas Ebenhan: <https://orcid.org/0000-0002-2038-7324>  
 Thavendran Govender: <https://orcid.org/0000-0003-2511-2503>

## REFERENCES

- Murray CJ, Ikuta KS, Sharara F, Swetschinski L, Aguilar GR, Gray A, Han C, Bisignano C, Rao P, Wool E. Global burden of bacterial antimicrobial resistance in 2019: a systematic analysis. *Lancet*. 2022;399(10325):629–655. [https://doi.org/10.1016/S0140-6736\(21\)02724-0](https://doi.org/10.1016/S0140-6736(21)02724-0).
- Vos T, Lim SS, Abbafati C, Abbas KM, Abbasi M, Abbasifard M, Abbasi-Kangevari M, Abbastabar H, Abd-Allah F, Abdelalim A, et al. Global burden of 369 diseases and injuries in 204 countries and territories, 1990–2019: a systematic analysis for the Global Burden of Disease Study 2019. *Lancet*. 2020;396(10258):1204–1222. [https://doi.org/10.1016/S0140-6736\(20\)30925-9](https://doi.org/10.1016/S0140-6736(20)30925-9).
- WHO. *The top 10 causes of death*. <https://www.who.int/news-room/fact-sheets/detail/the-top-10-causes-of-death> (accessed 02 December 2024).
- Miethke M, Pieroni M, Weber T, Bronstrup M, Hammann P, Halby L, Arimondo PB, Glaser P, Aigle B, Bode HB, et al. Towards the sustainable discovery and development of new antibiotics. *Nat Rev Chem*. 2021;5(10):726–749. <https://doi.org/10.1038/s41570-021-00313-1>.
- Ordonez AA, Wang H, Magombedze G, Ruiz-Bedoya CA, Srivastava S, Chen A, Tucker EW, Urbanowski ME, Pieterse L, Fabian Cardozo E, et al. Dynamic imaging in patients with tuberculosis reveals heterogeneous drug exposures in pulmonary lesions. *Nat Med*. 2020;26(4):529–534. <https://doi.org/10.1038/s41591-020-0770-2>.
- Annunziata S, Treglia G, Jamar F, Lauri C, Palestro CJ, Gheysens O, Glaudemans A. Nuclear medicine practice in the field of infection and inflammation imaging: a pragmatical survey. *Eur J Nucl Med Mol Imaging*. 2022;49(7):2113–2119. <https://doi.org/10.1007/s00259-022-05725-9>.
- Palestro CJ. Molecular Imaging of infection: the first 50 years. *Semin Nucl Med*. 2020;50(1):23–34. <https://doi.org/10.1053/j.semnuclmed.2019.10.002>.
- Palestro CJ, Clark A, Grady EE, Heiba S, Israel O, Klitzke A, Love C, Satheke M, Ted T, Yarbrough TL. Appropriate Use criteria for the use of nuclear medicine in musculoskeletal infection imaging. *J Nucl Med*. 2021;62(12):1815–1831. <https://doi.org/10.2967/jnumed.121.262579>.
- Akter A, Lyons O, Mehra V, Isenman H, Abbate V. Radiometal chelators for infection diagnostics. *Front Nucl Med*. 2023;2:1058388. <https://doi.org/10.3389/fnume.2022.1058388>.
- Gouws AC, Kruger HG, Gheysens O, Zeevaart JR, Govender T, Naicker T, Ebenhan T. Antibiotic-Derived radiotracers for positron emission tomography: nuclear or “unclear” infection imaging? *Angew Chem Int Ed*. 2022;61(45):e202204955. <https://doi.org/10.1002/anie.202204955>.

11. Alberto S, Ordonez AA, Arjun C, Aulakh GK, Beziere N, Dadachova E, Ebenhan T, Granados U, Korde A, Jalilian A, et al. The development and validation of radiopharmaceuticals targeting bacterial infection. *J Nucl Med.* 2023;64(11):1676–1682. <https://doi.org/10.2967/jnumed.123.265906>.
12. Ordonez AA, Sellmyer MA, Gowrishankar G, Ruiz-Bedoya CA, Tucker EW, Palestro CJ, Hammoud DA, Jain SK. Molecular imaging of bacterial infections: overcoming the barriers to clinical translation. *Sci Transl Med.* 2019;11(508):eaax8251. <https://doi.org/10.1126/scitranslmed.aax8251>.
13. Mota F, Ordonez AA, Firth G, Ruiz-Bedoya CA, Ma MT, Jain SK. Radiotracer development for bacterial imaging. *J Med Chem.* 2020;63(5):1964–1977. <https://doi.org/10.1021/acs.jmedchem.9b01623>.
14. Cross GB, O'Doherty J, Chang CC, Kelleher AD, Paton NI. Does PET-CT Have a Role in the Evaluation of Tuberculosis Treatment in Phase 2 Clinical Trials? *J Infect Dis.* 2024;229(4): 1229–1238. <https://doi.org/10.1093/infdis/jiad425>.
15. Signore A, Artiko V, Conserva M, Ferro-Flores G, Welling MM, Jain SK, Hess S, Satheke M. Imaging bacteria with radiolabelled probes: is it feasible? *J Clin Med.* 2020;9(8):2372. <https://doi.org/10.3390/jcm9082372>.
16. Polvoy I, Flavell RR, Rosenberg OS, Ohliger MA, Wilson DM. Nuclear imaging of bacterial infection: the state of the art and future directions. *J Nucl Med.* 2020;61(12):1708–1716. <https://doi.org/10.2967/jnumed.120.244939>.
17. Fura JM, Sabulski MJ, Pires MM. D-amino acid mediated recruitment of endogenous antibodies to bacterial surfaces. *ACS Chem Biol.* 2014;9(7):1480–1489. <https://doi.org/10.1021/cb5002685>.
18. Ohide H, Miyoshi Y, Maruyama R, Hamase K, Konno R. D-Amino acid metabolism in mammals: biosynthesis, degradation and analytical aspects of the metabolic study. *J Chromatogr B Analyt Technol Biomed Life Sci.* 2011;879(29):3162–3168. <https://doi.org/10.1016/j.jchromb.2011.06.028>.
19. Miyoshi Y, Koga R, Oyama T, Han H, Ueno K, Masuyama K, Itoh Y, Hamase K. HPLC analysis of naturally occurring free D-amino acids in mammals. *J Pharm Biomed Anal.* 2012;69:42–49. <https://doi.org/10.1016/j.jpba.2012.01.041>.
20. Hamase K, Morikawa A, Zaitzu K. D-Amino acids in mammals and their diagnostic value. *J Chromatogr B Analyt Technol Biomed Life Sci.* 2002;781(1–2):73–91. [https://doi.org/10.1016/S1570-0232\(02\)00690-6](https://doi.org/10.1016/S1570-0232(02)00690-6).
21. Friedman M, Levin CE. Nutritional and medicinal aspects of D-amino acids. *Amino Acids.* 2012;42(5):1553–1582. <https://doi.org/10.1007/s00726-011-0915-1>.
22. Cava F, de Pedro MA, Lam H, Davis BM, Waldor MK. Distinct pathways for modification of the bacterial cell wall by non-canonical D-amino acids. *EMBO J.* 2011;30(16):3442–3453. <https://doi.org/10.1038/emboj.2011.246>.
23. Cava F, de Pedro MA. Peptidoglycan plasticity in bacteria: emerging variability of the murein sacculus and their associated biological functions. *Curr Opin Microbiol.* 2014;18:46–53. <https://doi.org/10.1016/j.mib.2014.01.004>.
24. Alvarez L, Espallat A, Hermoso JA, de Pedro MA, Cava F. Peptidoglycan remodeling by the coordinated action of multispecific enzymes. *Microb Drug Resist.* 2014;20(3):190–198. <https://doi.org/10.1089/mdr.2014.0047>.
25. Horcajo P, de Pedro MA, Cava F. Peptidoglycan plasticity in bacteria: stress-induced peptidoglycan editing by noncanonical D-amino acids. *Microb Drug Resist.* 2012;18(3):306–313. <https://doi.org/10.1089/mdr.2012.0009>.
26. Cava F, Lam H, de Pedro MA, Waldor MK. Emerging knowledge of regulatory roles of D-amino acids in bacteria. *Cell Mol Life Sci.* 2011;68(5):817–831. <https://doi.org/10.1007/s00018-010-0571-8>.
27. Kuru E, Tekkam S, Hall E, Brun YV, Van Nieuwenhze MS. Synthesis of fluorescent D-amino acids and their use for probing peptidoglycan synthesis and bacterial growth in situ. *Nat Protoc.* 2015;10(1):33–52. <https://doi.org/10.1038/nprot.2014.197>.
28. Siegrist MS, Whiteside S, Jewett JC, Aditham A, Cava F, Bertozzi CR. (D)-Amino acid chemical reporters reveal peptidoglycan dynamics of an intracellular pathogen. *ACS Chem Biol.* 2013;8(3):500–505. <https://doi.org/10.1021/cb3004995>.
29. Kuru E, Hughes HV, Brown PJ, Hall E, Tekkam S, Cava F, de Pedro MA, Brun YV, VanNieuwenhze MS. In Situ probing of newly synthesized peptidoglycan in live bacteria with fluorescent D-amino acids. *Angew Chem Int Ed.* 2012;51(50):12519–12523. <https://doi.org/10.1002/anie.201206749>.
30. Gale RT, Brown ED. New chemical tools to probe cell wall biosynthesis in bacteria. *Curr Opin Microbiol.* 2015;27:69–77. <https://doi.org/10.1016/j.mib.2015.07.013>.
31. Hsu YP, Rittichier J, Kuru E, Yablonowski J, Pasciak E, Tekkam S, Hall E, Murphy B, Lee TK, Garner EC, et al. Full color palette of fluorescent d-amino acids for in situ labeling of bacterial cell walls. *Chem Sci.* 2017;8(9):6313–6321. <https://doi.org/10.1039/c7sc01800b>.
32. Koatle PC, Welling MM, Ndlovu H, Kgatle M, Mdanda S, Mdlophane A, Okem A, Takyi-Williams J, Satheke MM, Ebenhan T. Insights into peptidoglycan-targeting radiotracers for imaging bacterial infections: updates, challenges, and future perspectives. *ACS Infect Dis.* 2024;10(2):270–286. <https://doi.org/10.1021/acsinfecdis.3c00443>.
33. Polvoy I, Seo Y, Parker M, Stewart M, Siddiqua K, Manacs HS, Ravanfar V, Blecha J, Hope TA, Vanbrocklin H, et al. Imaging joint infections using D-methyl-(11)C-methionine PET/MRI: initial experience in humans. *Eur J Nucl Med Mol Imaging.* 2022;49(11):3761–3771. <https://doi.org/10.1007/s00259-022-05858-x>.
34. Muranaka Y, Mizutani A, Kobayashi M, Nakamoto K, Matsue M, Nishi K, Yamazaki K, Nishii R, Shikano N, Okamoto S, et al. Comparison of L- and D-amino acids for bacterial imaging in lung infection mouse model. *Int J Mol Sci.* 2022;23(5):2467. <https://doi.org/10.3390/ijms23052467>.
35. Renick PJ, Mulgaonkar A, Co CM, Wu CY, Zhou N, Velazquez A, Pennington J, Sherwood A, Dong H, Castellino L, et al. Imaging of actively proliferating bacterial infections by targeting the bacterial metabolic footprint with d-[5-(11)c]-glutamine. *ACS Infect Dis.* 2021;7(2):347–361. <https://doi.org/10.1021/acsinfecdis.0c00617>.
36. Parker MFL, Luu JM, Schulte B, Huynh TL, Stewart MN, Sriram R, Yu MA, Jivan S, Turnbaugh PJ, Flavell RR, et al. Sensing Living bacteria in vivo using d-alanine-derived (11)c radiotracers. *ACS Cent Sci.* 2020;6(2):155–165. <https://doi.org/10.1021/acscentsci.9b00743>.
37. Stewart MN, Parker MFL, Jivan S, Luu JM, Huynh TL, Schulte B, Seo Y, Blecha JE, Villanueva-Meyer JE, Flavell RR, et al. High enantiomeric excess in-loop synthesis of d-[methyl-(11)c]methionine for use as a diagnostic positron emission tomography radiotracer in bacterial infection. *ACS Infect Dis.* 2020;6(1):43–49. <https://doi.org/10.1021/acsinfecdis.9b00196>.
38. Wang C, Lin R, Yao S. Recent advances in (18)f-labeled amino acids synthesis and application. *Pharmaceutics.* 2022;14(10):2207. <https://doi.org/10.3390/pharmaceutics14102207>.
39. Scott PJH. Unnatural amino acids offer new hope for accurate bacterial infection PET imaging in prosthetic joint infection. *Eur J Nucl Med Mol Imaging.* 2022;49(11):3610–3612. <https://doi.org/10.1007/s00259-022-05857-y>.
40. Luurtsema G, Pichler V, Bongarzone S, Seimbille Y, Elsinga P, Gee A, Vercouillie J. EANM guideline for harmonisation on molar activity or specific activity of radiopharmaceuticals: impact on safety and imaging quality. *EJNMMI Radiopharm Chem.* 2021;6(1):34. <https://doi.org/10.1186/s41181-021-00149-6>.
41. Tsionou MI, Knapp CE, Foley CA, Munteanu CR, Cakebread A, Imberti C, Eykyn TR, Young JD, Paterson BM, Blower PJ, et al. Comparison of macrocyclic and acyclic chelators for gallium-68 radiolabelling. *RSC Adv.* 2017;7(78):49586–49599. <https://doi.org/10.1039/C7RA09076E>.
42. Mueller D, Breeman WA, Klette I, Gottschaldt M, Odparlik A, Baehre M, Tworowska I, Schultz MK. Radiolabeling of DOTA-like conjugated peptides with generator-produced (68)Ga and using NaCl-based cationic elution method. *Nat Protoc.* 2016;11(6):1057–1066. <https://doi.org/10.1038/nprot.2016.060>.
43. Dutta J, Chinthakindi PK, Arvidsson PI, Beatriz G, Kruger HG, Govender T, Naicker T, Albericio F. A facile synthesis of nodasa-functionalized peptide. *Synlett.* 2016;27(11):1685–1688.
44. Lauer JL, Fields CG, Fields GB. Sequence dependence of aspartimide formation during 9-fluorenylmethoxycarbonyl solid-phase peptide synthesis. *Lett Pept Sci.* 1995;1(4):197–205. <https://doi.org/10.1007/BF00117955>.
45. Subirós-Funosas R, El-Faham A, Albericio F. Aspartimide formation in peptide chemistry: occurrence, prevention strategies and the role of N-hydroxylamines. *Tetrahedron.* 2011;67(45):8595–8606. <https://doi.org/10.1016/j.tet.2011.08.046>.
46. Rossouw DD, Breeman WA. Scaled-up radiolabelling of DOTATATE with 68 Ga eluted from a SnO 2-based 68 Ge/68 Ga generator. *Appl Radiat Isot.* 2012;70(1):171–175. <https://doi.org/10.1016/j.apradiso.2011.07.016>.
47. Nelson BJB, Andersson JD, Wuest F, Spreckelmeyer S. Good practices for (68)Ga radiopharmaceutical production. *EJNMMI Radiopharm Chem.* 2022;7(1):27. <https://doi.org/10.1186/s41181-022-00180-1>.



48. Molavipordanjani S, Tolmachev V, Hosseinimehr SJ. Basic and practical concepts of radiopharmaceutical purification methods. *Drug Discov Today*. 2019;24(1):315–324. <https://doi.org/10.1016/j.drudis.2018.09.018>.
49. Meisenheimer M, Saenko Y, Eppard E. Chapter 2: Gallium-68: radiolabeling of radiopharmaceuticals for pet imaging - a lot to consider. In: Naqvi SAR, Imran MB (editors), *Medical Isotopes*. London: IntechOpen, 2021.
50. Velikyan I, Beyer GJ, Langstrom B. Microwave-supported preparation of (68)Ga bioconjugates with high specific radioactivity. *Bioconjug Chem*. 2004;15(3):554–560. <https://doi.org/10.1021/bc030078f>.
51. Talip Z, Favaretto C, Geistlich S, Meulen NPV. A step-by-step guide for the novel radiometal production for medical applications: case studies with (68)Ga, (44)Sc, (177)Lu and (161)Tb. *Molecules*. 2020;25(4):966. <https://doi.org/10.3390/molecules25040966>.
52. Maruk AY, Larenkov AA. Determination of ionic 68Ga impurity in radiopharmaceuticals: major revision of radio-HPLC methods. *J Radioanal Nucl Chem*. 2020;323(1):189–195. <https://doi.org/10.1007/s10967-019-06964-1>.
53. Le Roux JS. Optimization of production methods for gallium-68 PET radiopharmaceuticals in a hospital radiopharmacy. PhD thesis, Stellenbosch University, South Africa; 2020.
54. Larenkov AA, Maruk AY, Kodina GE. Intricacies of the determination of the radiochemical purity of 68Ga preparations: possibility of sorption of ionic 68Ga species on reversed-phase columns. *Radiochemistry*. 2018;60(6):625–633. <https://doi.org/10.1134/S1066362218060103>.
55. Ebenhan T, Chadwick N, Sathekge MM, Govender P, Govender T, Kruger HG, Marjanovic-Painter B, Zeevaart JR. Peptide synthesis, characterization and (68)Ga-radiolabeling of NOTA-conjugated ubiquitin fragments for prospective infection imaging with PET/CT. *Nucl Med Biol*. 2014;41(5):390–400. <https://doi.org/10.1016/j.nucmedbio.2014.02.001>.
56. Chen CJ, Chan CH, Lin KL, Chen JH, Tseng CH, Wang PY, Chien CY, Yu HM, Lin WJ. (68)Ga-labelled NOTA-RGD-GE11 peptide for dual integrin and EGFR-targeted tumour imaging. *Nucl Med Biol*. 2019;68–69:22–30. <https://doi.org/10.1016/j.nucmedbio.2018.11.003>.
57. Lindner S, Fiedler L, Wangler B, Bartenstein P, Schirrmacher R, Wangler C. Design, synthesis and in vitro evaluation of heterobivalent peptidic radioligands targeting both GRP- and VPAC(1)-Receptors concomitantly overexpressed on various malignancies - Is the concept feasible? *Eur J Med Chem*. 2018;155:84–95. <https://doi.org/10.1016/j.ejmech.2018.05.047>.
58. Hennion MC. Solid-phase extraction: method development, sorbents, and coupling with liquid chromatography. *J Chromatogr A*. 1999;856(1-2):3–54. [https://doi.org/10.1016/S0021-9673\(99\)00832-8](https://doi.org/10.1016/S0021-9673(99)00832-8).
59. Serdons K, Verbruggen A, Bormans G. The presence of ethanol in radiopharmaceutical injections. *J Nucl Med*. 2008;49(12):2071. <https://doi.org/10.2967/jnumed.108.057026>.
60. Klok RP, Windhorst AD. Residual solvent analysis by gas chromatography in radiopharmaceutical formulations containing up to 12% ethanol. *Nucl Med Biol*. 2006;33(7):935–938. <https://doi.org/10.1016/j.nucmedbio.2006.07.003>.
61. Price EW, Orvig C. Matching chelators to radiometals for radiopharmaceuticals. *Chem Soc Rev*. 2014;43(1):260–290. <https://doi.org/10.1039/C3CS60304K>.
62. Zhang Y, Hao M, Li L, Luo Q, Deng S, Yang Y, Liu Y, Fang W, Song E. Research progress of contrast agents for bacterial infection imaging in vivo. *Trends Anal Chem*. 2023;159:116916. <https://doi.org/10.1016/j.trac.2023.116916>.
63. Patamia V, Zagni C, Brullo I, Saccullo E, Coco A, Floresta G, Rescifina A. Computer-assisted design of peptide-based radiotracers. *Int J Mol Sci*. 2023;24(7):6856. <https://doi.org/10.3390/ijms24076856>.
64. Kleynhans J, Kruger HG, Cloete T, Zeevaart JR, Ebenhan T. In silico modelling in the development of novel radiolabelled peptide probes. *Curr Med Chem*. 2020;27(41):7048–7063. <https://doi.org/10.2174/0929867327666200504082256>.
65. Kleynhans J, Grobler AF, Ebenhan T, Sathekge MM, Zeevaart JR. Radiopharmaceutical enhancement by drug delivery systems: A review. *J Control Release*. 2018;287:177–193. <https://doi.org/10.1016/j.jconrel.2018.08.008>.
66. Mungan MD, Blin K, Ziemert N. ARTS-DB: a database for antibiotic resistant targets. *Nucleic Acids Res*. 2022;50(D1):D736–D740. <https://doi.org/10.1093/nar/gkab940>.
67. Bolcaen J, Kleynhans J, Nair S, Verhoeven J, Goethals I, Sathekge M, Vandevorde C, Ebenhan T. A perspective on the radiopharmaceutical requirements for imaging and therapy of glioblastoma. *Theranostics*. 2021;11(16):7911–7947. <https://doi.org/10.7150/thno.56639>.
68. Yoshimura F, Nikaido H. Diffusion of beta-lactam antibiotics through the porin channels of *Escherichia coli* K-12. *Antimicrob Agents Chemother*. 1985;27(1):84–92. <https://doi.org/10.1128/AAC.27.1.84>.
69. Lam H, Oh DC, Cava F, Takacs CN, Clardy J, de Pedro MA, Waldor MK. D-amino acids govern stationary phase cell wall remodeling in bacteria. *Science*. 2009;325(5947):1552–1555. <https://doi.org/10.1126/science.1178123>.
70. Mikulová MB, Mikus P. Advances in development of radiometal labeled amino acid-based compounds for cancer imaging and diagnostics. *Pharmaceuticals (Basel)*. 2021;14(2):167. <https://doi.org/10.3390/ph14020167>.
71. Shi S, Zhang L, Wu Z, Zhang A, Hong H, Choi SR, Zhu L, Kung HF. [(68)Ga]Ga-HBED-CC-DiAsp: A new renal function imaging agent. *Nucl Med Biol*. 2020;82–83:17–24. <https://doi.org/10.1016/j.nucmedbio.2019.12.005>.
72. Xia Y, Zeng C, Zhao Y, Zhang X, Li Z, Chen Y. Comparative evaluation of (68)Ga-labelled TATEs: the impact of chelators on imaging. *EJNMMI Res*. 2020;10(1):36. <https://doi.org/10.1186/s13550-020-00620-6>.
73. Mdlophane AH, Ebenhan T, Marjanovic-Painter B, Govender T, Sathekge MM, Zeevaart JR. Comparison of DOTA and NODAGA as chelates for 68Ga-labelled CDP1 as novel infection PET imaging agents. *J Radioanal Nucl Chem*. 2019;322(2):629–638. <https://doi.org/10.1007/s10967-019-06693-5>.